

X-ray Structural and Biological Evaluation of a Series of Potent and Highly Selective Inhibitors of Human Coronavirus Papain-like Proteases

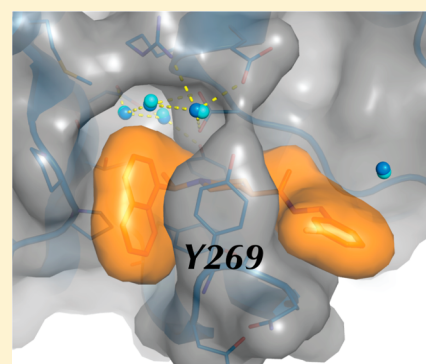
Yahira M. Báez-Santos,[†] Scott J. Barraza,[‡] Michael W. Wilson,[‡] Michael P. Agius,[‡] Anna M. Mielech,[§] Nicole M. Davis,[†] Susan C. Baker,[§] Scott D. Larsen,^{*,‡} and Andrew D. Mesecar^{*,†}

[†]Department of Biological Sciences, Purdue University, 915 W. State Street, West Lafayette, Indiana 47907, United States

[‡]Vahlteich Medicinal Chemistry Core and Department of Medicinal Chemistry, College of Pharmacy, University of Michigan, Ann Arbor, Michigan 48109, United States

[§]Department of Microbiology and Immunology, Loyola University Chicago Stritch School of Medicine, Maywood, Illinois 60153, United States

ABSTRACT: Structure-guided design was used to generate a series of noncovalent inhibitors with nanomolar potency against the papain-like protease (PLpro) from the SARS coronavirus (CoV). A number of inhibitors exhibit antiviral activity against SARS-CoV infected Vero E6 cells and broadened specificity toward the homologous PLP2 enzyme from the human coronavirus NL63. Selectivity and cytotoxicity studies established a more than 100-fold preference for the coronaviral enzyme over homologous human deubiquitinating enzymes (DUBs), and no significant cytotoxicity in Vero E6 and HEK293 cell lines is observed. X-ray structural analyses of inhibitor-bound crystal structures revealed subtle differences between binding modes of the initial benzodioxolane lead (**15g**) and the most potent analogues **3k** and **3j**, featuring a monofluoro substitution at para and meta positions of the benzyl ring, respectively. Finally, the less lipophilic bis(amide) **3e** and methoxyppyridine **5c** exhibit significantly improved metabolic stability and are viable candidates for advancing to in vivo studies.



■ INTRODUCTION

More than 10 years after the pandemic caused by the SARS (severe acute respiratory syndrome) coronavirus (CoV), no anticonviral regimens have been developed for the treatment of SARS-CoV or any other human coronaviruses (HCoV) infection. SARS-CoV was established as the causative agent of the fatal global outbreak of respiratory disease in humans during 2002–2003 that resulted in a case-fatality rate (CFR) of 11%.¹ In October 2012, the Centers for Disease Control and Prevention (CDC) added SARS-CoV to the select agents list of the Department of Health and Human Services (HHS). Among many aspects that make SARS-CoV a potential threat to the human population, the lack of effective vaccines or anticonviral drugs had a significant impact in its classification as a select agent. However, even with the most extensive preventive measures, the reemergence of SARS-CoV or other virulent human coronaviruses poses a continuing threat. A powerful reminder of this, as well as of the fatal repercussions of the interspecies transmission potential of CoVs, was brought to the forefront in September 2012 by the emergence of a new SARS-like respiratory virus (previously termed HCoV-EMC, now designated Middle East respiratory syndrome coronavirus, MERS-CoV).^{2,3} As in the case of SARS-CoV, the MERS-CoV is likely of zoonotic origin⁴ and closely related to bat coronaviruses from the *Betacoronavirus* genus (group 2).⁵

Reminiscent of the initial stages of SARS-CoV pandemic, global travel has contributed to the spread of MERS coronavirus, with a total of 178 laboratory-confirmed cases and a CFR of 43%.⁶ The infected individuals display SARS-like symptoms, including a severe respiratory infection (SRI), and sometimes exhibit an acute renal failure which is a unique signature of MERS infection.^{2b,7} Today, a total of 6 human coronaviruses are known, of which SARS-CoV and MERS-CoV are recognized as highly pathogenic with the potential for human-to-human transmission.⁸ Without an efficacious antiviral agent or vaccine, the prevention of current and emerging coronaviruses continues to rely strongly on public health measures to contain outbreaks. Therefore, research toward the development of anticonviral drugs continues to be of paramount importance.

The development of anticonviral drugs is challenging. Although a number of coronavirus proteins have been identified as potential drug targets,⁹ further development of drug candidates has been compromised by the general lack of antiviral data and biological evaluations, which can be done only in BSL-3 facilities with select agent certification for laboratories in the U.S. Two of the most promising drug targets are the SARS-CoV-encoded cysteine proteases, 3CLpro

Received: November 6, 2013

Published: February 25, 2014

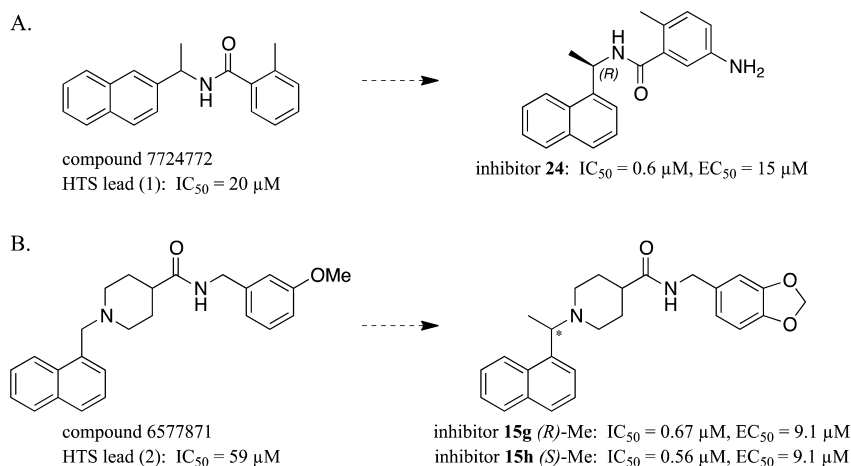


Figure 1. Chemical structures of previously characterized SARS-CoV PLpro inhibitors: (A) hit (1) from a primary HTS from which lead **24** was developed; (B) hit (2) from a primary HTS from which **15g** and **15h** were developed. The chiral center for the nearly equipotent isomers derived from hit **2** is indicated with an asterisk.

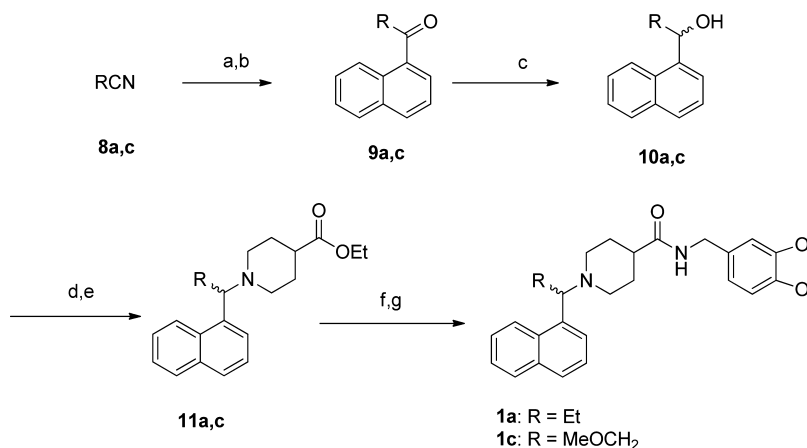
(chymotrypsin-like protease) and PLpro (papain-like protease). PLpro, in addition to playing an essential role during virus replication, is proposed to be a key enzyme in the pathogenesis of SARS-CoV. The well-established roles of PLpro enzymatic activities include processing of the viral polyprotein,¹⁰ deubiquitination¹¹ (the removal of ubiquitin), and deISGylation¹² (the removal of ISG15) from host-cell proteins. These last two enzymatic activities result in the antagonism of the host antiviral innate immune response.¹³ The SARS-CoV PLpro inhibitors (compounds **24**¹⁴ and **15g,h**¹⁵), previously identified in our lab via high-throughput screening (HTS), have low micromolar inhibitory potency with minimal associated cytotoxicity in SARS-CoV-infected Vero E6 cells and are therefore viable leads for the development of drug candidates (Figure 1). Detailed reports of the synthesis and biological evaluation of inhibitors **24**¹⁴ and **15g**¹⁵ and their X-ray structures in complex with SARS-CoV PLpro have been previously described.

Compounds **24**, **15h**, and **15g** share a number of chemical and structural features (Figure 1), including the presence of a naphthyl group adjacent to a stereogenic center containing a methyl group and a nitrogen-centered hydrogen bond (H-bond) donor (at a physiological pH). In addition, these leads share carboxamide linkers of opposite orientation to differentially substituted benzenoid groups. Structure–activity relationships (SARs) have shown that in both inhibitor subtypes the naphthyl ring is optimally substituted at C-1 and the presence of the methyl group at the aforementioned stereogenic center is important for potency.^{14,15} Interestingly, SARS-CoV PLpro exhibited significant stereopreference for the (*R*)-enantiomer of **24** ($IC_{50} = 0.6 \mu M$, $EC_{50} = 15 \mu M$),¹⁴ while minimal stereochemical selectivity was observed between enantiomers (*R*)-**15g** and (*S*)-**15h** (IC_{50} values of 0.67 and 0.56 μM , respectively; EC_{50} of 9.1 μM for both).¹⁵

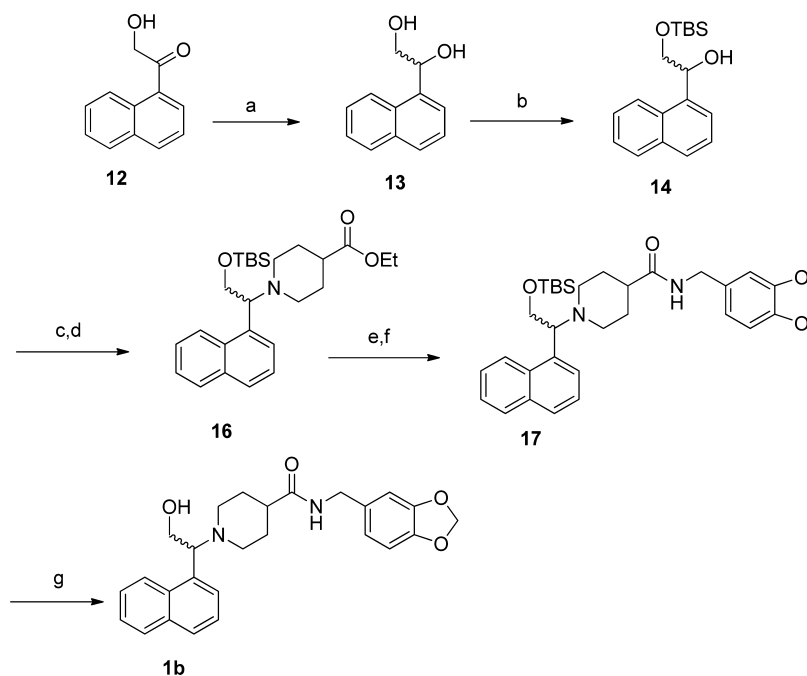
The structural bases for the high binding affinity of inhibitors **24** and **15g,h** are also quite similar. The X-ray crystal structures of PLpro–**24** and PLpro–**15g** complexes revealed several hydrophobic interactions resultant of the highly hydrophobic naphthyl ring and few hydrogen bonds.^{13a,14} In addition, significant conformational changes within the active site are prominent between the apo¹⁶ and inhibitor-bound structures.^{14,15} Specifically, there is a highly mobile β -turn/loop (Gly₂₆₇–Gly₂₇₂) adjacent to the active site that closes upon

inhibitor binding, thereby changing the orientation of the enzyme's backbone to allow for H-bonding with the inhibitor's core. However, relative to the conformation adopted with the smaller inhibitor **24**, compound **15g** requires a different and slightly more opened conformation to accommodate the longer piperidine-4-carboxamide scaffold and the bulkier 1,3-benzodioxole ring.

Because the antiviral potencies of these SARS-CoV PLpro inhibitors are likely not yet sufficient to make them therapeutically viable, further optimization of their inhibitory potencies, as well as physicochemical properties, is necessary. Toward this goal, we utilized our previous SAR analysis and the X-ray structure of compound **15g** in complex with SARS-CoV PLpro to develop a second generation of PLpro inhibitors. Here, we disclose SAR of a new series of potent SARS-CoV PLpro inhibitors, their selectivity, antiviral efficacy, biological evaluation, and a detailed report of the molecular interactions between SARS-CoV PLpro and inhibitors **3k** and **3j** aided by X-ray crystallographic studies. Compound **3k** was established to be the most potent SARS-CoV PLpro inhibitor identified thus far in vitro. Furthermore, this compound displayed effective perturbation of SARS-CoV replication in Vero E6 cells while displaying low cytotoxicity and high selectivity for SARS-CoV PLpro over human homologue enzymes. The improved resolution of the SARS-CoV PLpro–**3k** and PLpro–**3j** X-ray structures revealed novel factors accounting for the observed high binding affinities of the piperidine-containing compounds and the previously elusive molecular contributions of the benzyl substituent of the carboxamide. Therefore, our data highlight **3k**, as well as two slightly less potent but more metabolically stable analogues **3e** and **5c**, as good candidates for advancing to preclinical evaluations. In addition, we demonstrate the effective inhibition of PLP2 from HCoV-NL63, a potentially fatal pathogen in children and elderly, by compound **3k** and related analogues. Importantly, these compounds may also present an opportunity for the development of broader-spectrum antiviral drugs against infections caused by both SARS-CoV and HCoV-NL63.

Scheme 1. Synthesis of α -Substituted Naphthyl Analogues^a

^aReagents and conditions: (a) 1-naphthyl-MgBr, ether, rt; (b) Aq HCl; (c) LAH, THF, rt; (d) Ms₂O, DIEA, DCM, 0 °C; (e) ethyl isonipecotate, rt; (f) aq NaOH, EtOH, THF; (g) piperonylamine, EDCl, HOBT, DIEA, rt.

Scheme 2. Synthesis of α -Hydroxymethyl Analogue 1b^a

^aReagents and conditions: (a) LAH, THF, rt; (b) TBSCl, imidazole, ether, rt; (c) Ms₂O, DIEA, DCM, rt; (d) ethyl isonipecotate, rt; (e) aq NaOH, EtOH, 40 °C; (f) piperonylamine, EDCl, HOBT, DIEA, rt; (g) CsF, aq ACN, rt.

RESULTS AND DISCUSSION

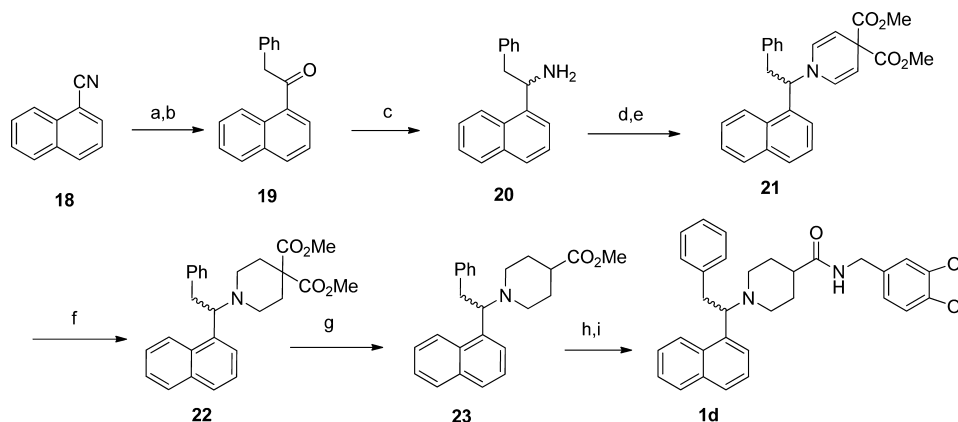
Chemistry. The preparation of analogues 1a–d bearing substitution off the α -methyl group is summarized in Schemes 1–3.

The appropriate nitriles 8a,c were treated with 1-naphthyl Grignard reagent, and the intermediary imines were hydrolyzed to the ketones 9a,c under acidic conditions (Scheme 1).¹⁷ The ketones were then reduced by the action of LAH to the alcohols 10a,c, which were mesylated and displaced by treatment with ethyl isonipecotate to provide the amino esters 11a,c. Saponification to the carboxylic acids was followed by coupling with piperonylamine to give final racemic analogues 1a,c.

A similar displacement strategy was employed to obtain hydroxyl analogue 1b (Scheme 2). Hydroxy ketone 12¹⁸ was

reduced with LAH to the diol 13, and the primary alcohol was selectively protected as the *tert*-butyldimethylsilyl (TBS) ether to give 14. The free secondary alcohol was mesylated and displaced by ethyl isonipecotate, and the resulting amino ester 16 was hydrolyzed to the corresponding acid and coupled with piperonylamine to provide the TBS-protected compound 17. The silyl ether was removed with CsF to afford the desired hydroxy analogue 1b.

The displacement route used in Schemes 1 and 2 was not successful with the more hindered phenyl analogue 1d, so we had to employ the lengthier approach previously reported by Ghosh et al. (Scheme 3).¹⁵ 1-Naphthonitrile 18 was treated with benzylmagnesium chloride, and the resulting imine was hydrolyzed under acidic conditions to the ketone 19. Reductive amination as previously described¹⁹ provided amine 20. This

Scheme 3. Synthesis of α -Phenylmethyl Analogue 1d^a

^aReagents and conditions: (a) BnMgCl , ether, rt; (b) 1 M HCl , ether, 90 °C; (c) CH_3ONH_2 , pyridine, rt; then $\text{BH}_3\text{-THF}$, 80 °C;¹⁸ (d) dimethyl 2,2-bis((1,3-dioxolan-2-yl)methyl)malonate, HCl/THF ; (e) **20**, rt, 20 h; (f) H_2 , Pd/C , 40 psi, rt; (g) NaCN , DMF , 145 °C; (h) 1 M aq NaOH , EtOH , 60 °C; (i) piperonylamine, EDCI , HOBt , DIEA , rt.

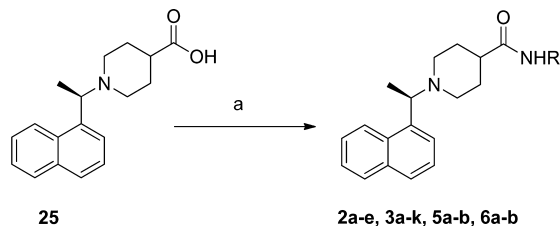
amine was then condensed with the bis-aldehyde derived from dimethyl 2,2-bis((1,3-dioxolan-2-yl)methyl)malonate to give the dihydropyridine dimethyl ester **21**, which was readily reduced to the piperidine **22** by heterogeneous hydrogenation. The diester was converted into the monoester **23** by the Krapcho method and was subsequently hydrolyzed to the acid and coupled with piperonylamine to give the desired analogue **1d**.

Preparation of (*R*)-amide analogues is summarized in Scheme 4. The starting (*R*)-1-(1-(naphthalen-1-yl)ethyl)-

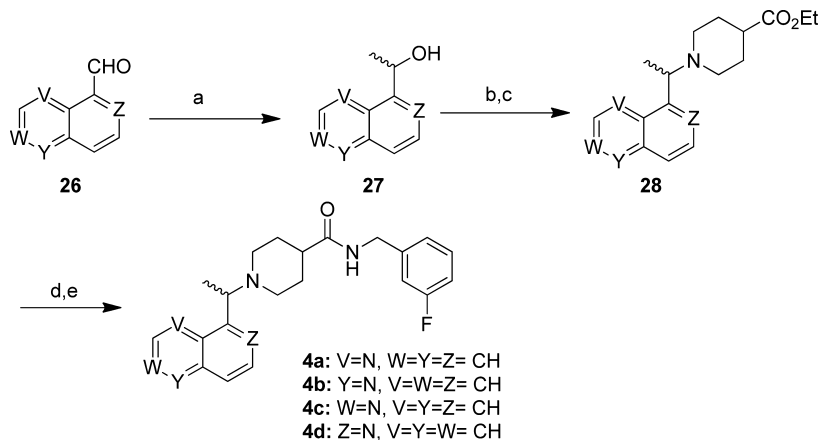
piperidine-4-carboxylic acid **25** was prepared according to the method of Ghosh et al.¹⁵ Coupling of the acid to various arylmethylamines and aryethylamines was effected either by EDCI in the presence of DIEA or by the uronium-based coupling reagent HATU .

The racemic quinolinyl and isoquinolinyl analogues (**4a–c**) were generated from the corresponding aldehydes **26a–c** by treatment with methylmagnesium chloride to give the methylcarbinols **27a–c** (Scheme 5). Alternatively, carbinol **27d** was prepared from 1-cyanoisoquinoline by addition of methylmagnesium chloride followed by sodium borohydride reduction of the resulting ketone, as described in the Experimental Section. Displacement of the corresponding mesylates with ethyl isonipecotate afforded esters **28a–d** (Scheme 5). Saponification followed by EDCI -mediated coupling with 4-fluorobenzylamine provided the final amides **4a–d**.

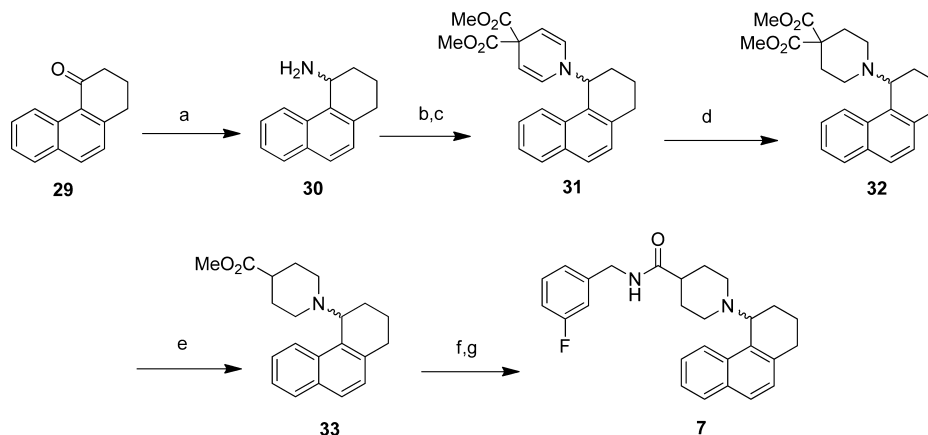
Conformationally restricted analogue **7** was prepared as outlined in Scheme 6. Reductive amination of ketone **29** with ammonium acetate and sodium cyanoborohydride provided amine **30** in quantitative yield. Conversion to piperidine ester **33** was effected with a three-step sequence analogous to that

Scheme 4. General Synthesis of Amide Analogues^a

^aReagents and conditions: (a) RNH_2 , EDCI or HATU , DIEA .

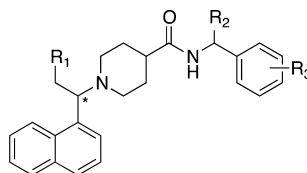
Scheme 5. Synthesis of Quinolinyl- and Isoquinolinylamides^a

^aReagents and conditions: (a) MeMgCl , THF , -78 °C; (b) Ms_2O , DIEA , DCM ; (c) ethyl isonipecotate, DCM , rt; (d) 1 M NaOH , MeOH ; (e) EDCI , HOBt , DIEA , 3-fluorobenzylamine, THF .

Scheme 6. Synthesis of Conformationally Restricted Analogue 7^a

^aReagents and conditions: (a) NaBH₃CN, NH₄OAc, ¹PrOH, reflux, 44 h; (b) dimethyl 2,2-bis((1,3-dioxolan-2-yl)methyl)malonate, HCl/THF; (c) 30, NaHCO₃, rt, 72 h; (d) H₂, PtO₂, EA, 40 psi, 5 h; (e) NaCN, DMF, reflux, 16 h; (f) aq LiOH, THF/MeOH, rt; (g) 3-fluorobenzylamine, EDCI, HOBT, DIEA, rt, 16 h.

Table 1. In Vitro Analysis of SARS-CoV PLpro Inhibition by 15g and Derivatives



compd	isomer ^a	R ₁	R ₂	R ₃	IC ₅₀ (μM) ^b
15g	R	H	H	3,4-O-CH ₂ -O	0.67 ± 0.03
1a	R,S	Me	H	3,4-O-CH ₂ -O	17.2 ± 2.0
1b	R,S	OH	H	3,4-O-CH ₂ -O	32.0 ± 4.5
1c	R,S	OMe	H	3,4-O-CH ₂ -O	>100
1d	R,S	Ph	H	3,4-O-CH ₂ -O	>100
2a	R	H	H	H	2.2 ± 0.1
2b	R	H	(R)-Me	H	13.5 ± 1.2
2c	R	H	(S)-Me	H	12.7 ± 0.3
2d	R	H	(R)-CH ₂ -OMe	H	18.0 ± 1.9
2e	R	H	(S)-CH ₂ -OMe	H	1.9 ± 0.1
3a	R	H	H	4-Et	0.47 ± 0.01
3b	R	H	H	4-CO-NH-Me	0.60 ± 0.02
3c	R	H	H	3-CO-NH-Me	0.63 ± 0.01
3d	R	H	H	4-NH-CO-Me	5.7 ± 0.5
3e	R	H	H	3-NH-CO-Me	0.39 ± 0.01
3f	R	H	H	3-CH ₂ -NH-CO-Me	20.4 ± 1.2
3g	R	H	H	3-Cl	27.2 ± 4.1
3h	R	H	H	4-Cl	0.58 ± 0.02
3i	R	H	H	3,4-diF	29.2 ± 2.1
3j	R	H	H	4-F	0.49 ± 0.01
3k	R	H	H	3-F	0.15 ± 0.01

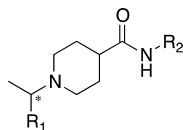
^aChiral center. ^bValues are reported as mean ± standard deviation based on a minimum of triplicate measurements.

employed in Scheme 3. Saponification with LiOH in a mixture (3:1:1) of THF/MeOH/H₂O furnished the free acid. Finally amide coupling with 3-fluorobenzylamine, EDCI, HOBT, and DIEA led to the production of the target analogue 7. It is worth noting that the shorter ethyl isonipecotate displacement route used in Schemes 1, 2, and 5 was not successful with the mesylate derived from reduction/mesylation of 29, presumably because of excessive steric hindrance.

Structure–Activity Relationship Analysis. Compound 15g is a competitive inhibitor of SARS-CoV PLpro that displays

potent enzymatic inhibition (IC₅₀ = 0.67 μM) and low micromolar antiviral activity against SARS-CoV. It evolved from a small SAR study on the HTS hit 2 (Figure 1) and is therefore an attractive lead for the development of anti-SARS drug candidates.¹⁵ Compound 15g is composed of the central piperidine-4-carboxamide core decorated with 1-naphthalenylethyl and 1,3-benzodioxolymethyl substituents at the piperidinyl and carboxamide nitrogens, respectively. Previous SAR has established the preference for the 1-naphthyl over the 2-naphthyl substitution pattern and the requirement of a single

Table 2. Structures and Activities of 3k Variants, Exploring Bioisosteric Replacements and Scaffold Perturbation



compd	isomer ^a	R ₁	R ₂	IC ₅₀ (μM) ^b
3k	R	1-naphthyl	3-F-Ph-CH ₂	0.15 ± 0.01
4a	R,S	8-quinolinyl	3-F-Ph-CH ₂	7.0 ± 0.7
4b	R,S	5-quinolinyl	3-F-Ph-CH ₂	4.5 ± 0.2
4c	R,S	5-isoquinolinyl	3-F-Ph-CH ₂	6.8 ± 0.3
4d	R,S	1-isoquinolinyl	3-F-Ph-CH ₂	30.8 ± 2.6
5a	R	1-naphthyl	3-pyridinyl-CH ₂	26.3 ± 2.3
5b	R	1-naphthyl	4-pyridinyl-CH ₂	18.3 ± 0.9
5c	R	1-naphthyl	2-methoxy-4-pyridinyl-CH ₂	0.35 ± 0.02
6a	R	1-naphthyl	4-Cl-Ph-CH ₂ CH ₂	1.6 ± 0.3
6b	R	1-naphthyl	3-F-Ph-CH ₂ CH ₂	1.9 ± 0.1

^aChiral center. ^bValues are reported as mean ± standard deviation based on a minimum of triplicate measurements.

methyl substituent at the methylene linker for effective inhibition (when compared to both unsubstituted and *gem*-dimethyl derivatives), with minimal stereochemical preference. X-ray crystallographic studies of the SARS-CoV PLpro–15g complex show that the methyl group of the (*R*)-enantiomer extends into a small pocket that has both hydrophobic and polar features and is filled with water molecules. To explore the dimensions and availability of this pocket to substituents as well as H-bond opportunities, the first set of analogues explores the incorporation of larger or polar substituents (**1a**, -Me; **1b**, -OH; **1c**, -OMe; **1d**, -Ph) at the methyl group (position R₁ in Table 1). Addition of substituents to R₁ resulted in higher IC₅₀ values for all substitutions, and loss of inhibitory potency was proportional to substituent size. These trends indicate that the corresponding pocket might be less accessible than predicted by the crystal structure, with no clear opportunities for extra H-bonding or lipophilic interactions. It also appears that the potential entropic gain by displacing the water molecules with larger R₁ groups is not achieved likely because of a larger enthalpic penalty of breaking the H-bonds formed between these water molecules and Asp₁₆₅, Arg₁₆₇, Tyr₂₇₄, Thr₃₀₂, and Asp₃₀₃. As a result, unlike the previously reported predictions by fragment mapping program (FTMap) in which all water molecules were removed before computational analyses,²⁰ here we demonstrate experimentally that this pocket is unlikely to provide any extra ligand-binding sites or room for larger substituents.

We next examined the effect of incorporating substituents at the benzylic position R₂ to form a second stereogenic carbon, using unsubstituted compound **2a** (IC₅₀ = 2.2 ± 0.1 μM) as the comparator. Diastereoisomeric epimers **2b** and **2c**, with a methyl group at R₂, decreased the inhibitory activity by a comparable extent (IC₅₀ of 13.5 ± 1.2 and 12.7 ± 0.3 μM, respectively), indicative of a steric clash with SARS-CoV PLpro. Interestingly, a 10-fold stereopreference was observed for (*S*)-methoxymethyl **2e** (IC₅₀ = 1.9 ± 0.1 μM), compared to epimeric **2d** (IC₅₀ = 18.0 ± 1.9 μM), which could be indicative of a H-bond in that region or simply the ability of the more active enantiomer **2e** to retain the methoxy in a solvent-exposed environment, thereby avoiding a desolvation penalty. However, because the most active analogue in this series, **2e**, did not surpass the effectiveness of the initial unsubstituted compound, **2a**, we surmise that substitutions at position R₂ do

not engage the active site of the enzyme in favorable interaction and are therefore unlikely to lead to activity improvement.

Previous SAR studies on the aromatic substitution pattern of the benzyl group were limited to *m*- and *p*-methoxy analogues, which were as potent as the lead benzodioxolane analogue, **15g**.¹⁵ In the X-ray structure of the SARS-CoV PLpro–15g complex, one of the 1,3-dioxolane oxygens is within 3 Å of the Gln₂₇₀ side chain amide nitrogen, suggesting the potential for forming an H-bond. However, because of the poor electron density for the Gln₂₇₀ side chain, the oxygen's contribution to inhibitory potency was uncertain.¹⁵ Therefore, we mutated Gln₂₇₀ to an alanine, glutamate, or aspartate residue and purified the mutant enzymes and determined the IC₅₀ values with **15g**. We found that the IC₅₀ values for the mutant enzymes are the same as for wild type SARS-CoV PLpro, indicating that Gln₂₇₀ does not contribute to the binding of **15g** via interaction with the dioxolane ring (data not shown). As observed with compound **2a**, removal of the dioxolane ring from **15g** results in a ~3-fold decrease in potency, suggesting that the dioxolane group provides a significant contribution to inhibitory potency but not through interaction with Gln₂₇₀. Therefore, to elucidate the nature of interactions provided by the 1,3-benzodioxole group, benzene ring derivatives with diverse substituents at position R₃ were explored.

The incorporation of a *p*-ethyl group at R₃ (**3a**) had a more than 4-fold improvement in potency over unsubstituted prototype **2a**, surpassing that of the dioxolane lead (**15g**). A comparable effect was achieved with both *p*- and *m*-methylcarboxamide derivatives **3b** (IC₅₀ = 0.60 ± 0.02 μM) and **3c** (IC₅₀ = 0.63 ± 0.01 μM) respectively displaying both H-bonding donors and acceptors. Reversal of the amide direction to the acetamido group resulted in significantly differing activity levels for para and meta positional isomers **3d** (IC₅₀ = 5.7 ± 0.5 μM) and **3e** (IC₅₀ = 0.39 ± 0.01 μM), respectively. Further extension of the acetamido group from the meta position, favored in the previous pair, dramatically decreases activity of the corresponding derivative (**3f**, IC₅₀ = 20.4 ± 1.2 μM). A reversal in the meta vs para trend is seen with the corresponding pair of chloro derivatives **3g** (IC₅₀ = 27.2 ± 4.1 μM) and **3h** (IC₅₀ = 0.58 ± 0.01 μM), with the halogen tolerated only at the para position. Finally, derivatives **3j** and **3k**, featuring the monofluoro substitution at para and meta positions, respectively, displayed a significant improvement

over the parental **2a** structure, with the 3-fluorobenzyl variant possessing a more than 10-fold higher activity level ($IC_{50} = 0.15 \pm 0.01 \mu M$). Surprisingly, 3,4-difluoro substitution in **3i** ($IC_{50} = 29.2 \pm 2.1 \mu M$) had a significantly detrimental effect, decreasing the inhibitory potency by ~ 200 -fold when compared to **3k**. In general, neither steric nor electronic factors can be invoked to rationalize systematically the effects of the substitution pattern at R_3 and R_4 on the inhibitory activity, with groups as diverse as 1,3-dioxolane, 4-ethyl, 3- and 4-carboxamido, 3-acetamido, 3- and 4-fluoro, and 4-chloro achieving a similar level of activity, despite presenting a wide range in polarity, size, and H-bonding capacity. Significantly, the monosubstitution at the meta position with the smallest and yet the most electron-withdrawing fluoro group, capable of inducing dramatic polarization effects in the π -system of the associated benzene ring, resulted in the most potent SARS-CoV PLpro inhibitor identified thus far.

In an attempt to improve the solubility of our most potent compound, **3k**, the bioisosteres of naphthalene and benzene (quinoline and pyridine, respectively) were exploited by synthesizing corresponding derivatives (Table 2). A detrimental effect on activity is observed upon replacement of the naphthyl ring system by quinolines (**4a**, $IC_{50} = 7.0 \pm 0.7 \mu M$ and **4b**, $IC_{50} = 4.5 \pm 0.2 \mu M$) and isoquinolines, (**4c**, $IC_{50} = 6.8 \pm 0.3 \mu M$ and **4d**, $IC_{50} = 30.8 \pm 2.6 \mu M$), all tested as racemates. The replacement of the phenyl ring in the **2a** prototype by the isosteric 3- and 4-pyridinyls (**5a**, $IC_{50} = 26.3 \pm 2.3 \mu M$ and **5b**, $IC_{50} = 18.3 \pm 0.9 \mu M$) decreased potency by over an order of magnitude. Interestingly, the activity was rescued by the addition of a 3-methoxy group to the 4-pyridinyl ring of the **5b** analogue (**5c**, $IC_{50} = 0.35 \pm 0.02 \mu M$), confirming the benefit of having a H-bonding group at C-3 of the aromatic ring. We tested whether Gln₂₇₀ was involved in an interaction with compound **5c** by determining its IC_{50} value with each of the SARS PLpro mutant enzymes (Gln₂₇₀Ala, Gln₂₇₀Asp, and Gln₂₇₀Glu). We observed no differences in the IC_{50} values within experimental error, indicating that no significant interaction is involved (data not shown). Analysis of the active site for other potential hydrogen-bonding residues produced no obvious candidates.

Extending the separation of the two aromatic centers in compounds **3h** and **3k** by one carbon atom resulted in weakening of inhibition activity in corresponding variants **6a** ($IC_{50} = 1.6 \pm 0.3 \mu M$) and **6b** ($IC_{50} = 1.9 \pm 0.1 \mu M$). The effect is surprisingly minor, considering the nature of this perturbation, and is perhaps indicative of a significant amount of flexibility in the active site of SARS-CoV PLpro in the region bound by the benzene moiety.

Finally, tricyclic analogue **7** was prepared as a conformationally restricted analogue of our most potent inhibitor **3k** (Figure 2). It was designed to lock the conformation of the bond joining C-1 of the naphthyl ring to the piperidylethyl group to that observed in the X-ray structure of the SARS-CoV PLpro–**15g** complex. This modification, however, led to a significant loss of activity ($IC_{50} = 5.1 \pm 0.5 \mu M$). These results suggest an inhibitor-induced-fit mechanism of association, in which the size and conformational freedom of compound **3k** allow the optimal fit to be achieved.

X-ray Structural Analyses of SARS-CoV PLpro Bound to 3k and 3j and Comparison to 15g. To gain structural insight into the enhanced potency of compound **3k**, SARS-CoV PLpro was cocrystallized as a complex with **3k** (PDB code 4OW0) and **3j** (PDB code 4OVZ) using an approach similar to

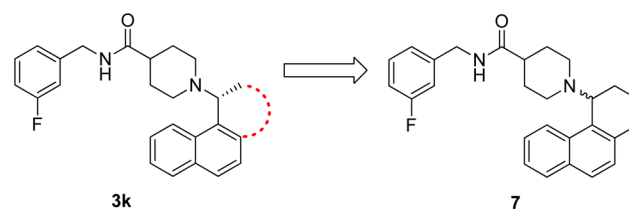


Figure 2. Chemical structure of compound **7**. The conformationally restricted analogue **7** was designed to lock the conformation of compound **3k** to the conformation observed in the X-ray crystal structure of SARS-CoV PLpro bound to **15g**.

that for **15g**.¹⁵ Crystals for each SARS-PLpro complex resulted after screening over 3000 crystallization conditions for diffraction quality crystals. Complete X-ray data sets were collected for the SARS-CoV PLpro–**3k** and PLpro–**3j** complexes to resolutions of 2.1 and 2.5 Å, respectively (Table 3). Both SARS-CoV PLpro–inhibitor complexes crystallized in space group C2 and contained two monomers per asymmetric unit.

After identification of a molecular replacement solution and performance of initial rounds of refinement of the SARS-CoV PLpro structural model in the absence of any ligand or water, strong ($>3\sigma$) residual electron density was observed in $F_o - F_c$ maps for both **3k** and **3j** in the active sites of each monomer within the asymmetric unit. The strong and continuous electron density for the inhibitors allowed for their unequivocal positioning and modeling within the ligand-binding site (Figure 3a and Figure 3b). Both **3k** and **3j** bind to the SARS-CoV PLpro active site in the same orientation (Figure 3c and Figure 3d).

As described previously for compounds **24** and **15g**, compounds **3k** and **3j** bind adjacent to the active site at the enzyme S3–S4 subsites^{14,15} (Figure 3c and Figure 3d), exclusive of any interactions with the catalytic triad (Cys₁₁₂–His₂₇₃–Asp₂₈₇). Upon inhibitor binding, the β -turn/loop (Gly₂₆₇–Gly₂₇₂) containing Tyr₂₆₉ adopts a closed conformation via an induced-fit mechanism to interact with the inhibitors. This enables the formation of a 3 Å H-bond between the backbone carbonyl of Tyr₂₆₉ and the carboxamide nitrogen of the inhibitors. An additional and important interaction is observed between the piperidine ring nitrogen and the side chain carboxylate of Asp₁₆₅. The puckering of the piperidine ring positions the cationic nitrogen within a distance of 2.8 Å from an oxygen of the carboxylate of Asp₁₆₅, thereby forming a charge-to-charge mediated H-bond.

A structural superimposition of the two SARS-CoV PLpro–**3k** and PLpro–**3j** complexes (Figure 3e) shows that the 1-naphthyl rings align identically and that they pack against the two tandem prolines, Pro₂₄₈ and Pro₂₄₉, in a hydrophobic pocket formed by the side chains of the prolines, Tyr₂₆₅, Tyr₂₆₉, and Thr₃₀₂ (Figure 3c and Figure 3d). This pocket orients the (R)-methyl group into a small cavity lined by hydrophobic and hydrophilic side chains wherein some H-bond opportunities exist with the side chains of Asp₃₀₃, Thr₃₀₂, and Tyr₂₇₄. The enhanced resolution of PLpro–**3k** and PLpro–**3j** complex compared to PLpro–**15g** complex allowed for the better placement of three conserved water molecules that are present within this cavity (Figure 3e). The presence of these water molecules increases the polarity and decreases the effective size of the otherwise larger and mostly hydrophobic cavity. This smaller cavity explains our observed SAR with hydrophobic or polar extensions at the (R)-methyl (position R_1 in Table 1)

Table 3. Data Collection and Refinement Statistics

	3k	3j
	Data Collection	
beamline	21-ID-F	21-ID-F
wavelength (Å)	0.98	0.98
space group	C2	C2
unit cell dimensions		
<i>a</i> , <i>b</i> , <i>c</i> (Å)	119.4, 74.4, 98.3	119.8, 73.5, 98.3
α , β , γ (deg)	90, 104, 90	90, 104, 90
resolution (Å)	100–2.10 (2.14–2.10)	100–2.50 (2.54–2.50)
no. of reflections observed	514232	743761
no. of unique reflections	49274	29021
R_{merge} (%)	6.2 (52.3)	6.5 (69.6)
$I/\sigma I$	20.6 (1.9)	19.3 (1.8)
% completeness	98.6 (96.1)	99.8 (100)
redundancy	4.7 (3.9)	4.2 (4.2)
	Refinement	
resolution range (Å)	31.79–2.10	35.75–2.50
no. of reflections in working set	42169	24909
no. of reflections in test set	2134 (5.1%)	1265 (5.1%)
R_{work} (%)	0.18	0.19
R_{free} (%)	0.20	0.24
average <i>B</i> factor (Å ²)	39	37
rmsd from ideal geometry		
bond length (Å)	0.022	0.026
bond angle (deg)	1.5	1.7
Ramachandran plot		
most favored (%)	94.0	92.6
allowed (%)	4.8	5.6
disallowed (%)	1.2	1.8

whereby the larger groups were all detrimental to binding affinity. These observations suggest that the potential entropic gain in binding energy by displacement of the water molecules cannot be achieved by incorporation of larger or polar substituents, as the enthalpy necessary to break the H-bonds between water molecules and the side chains must be too large to overcome.

A superimposition of PLpro in complex with **15g**, **3k**, and **3j** is shown in Figure 3f. As discussed above, previous structural and computational analyses of the **15g**-bound structure showed that the 1,3-benzodioxole moiety can move within 3 Å of the amide nitrogen of Gln₂₇₀ side chain. However, mutation of Gln₂₇₀ to Ala, Glu, or Asp showed no significant change in inhibitory potency when tested against **15g**, **3k**, and **3j**, indicative of no H-bond interactions with the side chain of Gln₂₇₀. Interestingly, while the superimposition between PLpro–**15g**, PLpro–**3k**, and PLpro–**3j** complexes shows a near perfect overlap of the 1-naphthyl rings, there is a 1 Å difference in the position of the carboxamide nitrogen of **15g** when compared to **3k** and **3j**. This causes a slight tilt on the orientations of the benzene rings to allow for the accommodation of the different benzene substituents. As a result, we conclude that the slightly enhanced inhibitory activity of compound **3k** compared to **3j** and **15g** is due to its ability to form collectively stronger van der Waals' interactions between the *m*-fluorobenzene and the side chain of Tyr₂₆₉, and slightly stronger interactions with the backbone oxygen atoms of Tyr₂₆₉ and Gln₂₇₀ (Figure 3f).

Assessing Potency and Selectivity of SARS-CoV PLpro Inhibitors to Human and Viral USP Homologues. The development of an enzyme inhibitor with broad-spectrum

specificity is an attractive approach for the treatment of infections caused by current and future-emerging human coronaviruses. However, to avoid drug-induced toxicity and potential side effects, it is crucial to maintain high inhibitory potency without cross-reactivity of critical homologues, the cellular deubiquitinating enzymes (DUBs). First, to assess compound selectivity, a set of the most potent analogues were tested against a panel of human DUBs, including representative ubiquitin specific proteases (USPs) with structural similarity to PLpro, along with the human cysteine proteases caspase 3 and cathepsin K (Table 4). Compounds were tested at 31 μM. If the inhibitory activity was less than 10%, no inhibition is reported. If the inhibitory activity was between 10% and 15% or between 15% and 20%, then IC₅₀ values of >100 or 31 μM are reported. Importantly, we can detect no significant inhibition of the human DUBs or cysteine protease enzymes tested above 20% at 31 μM, indicating that these PLpro inhibitors are selective and are unlikely to have significant off-target activity.

Next, we evaluated the potential of this set of analogues for the development of broader-spectrum coronaviral inhibitors. All of the analogues in Tables 1 and 2 were counterscreened against the viral orthologue PLP2 enzyme from the human coronavirus NL63 (HCoV-NL63), a member of the α -coronaviruses. HCoV-NL63 is one of the causative agents of croup in children, and infection can result in hospitalization.²¹ Currently there are no specific treatments for individuals infected with HCoV-NL63. For those analogues that showed >30% inhibition at a single dose concentration of 100 μM, full dose response curves of HCoV-NL63 PLP2 inhibition versus increasing compound concentration up to 100 μM were determined. Six compounds, including compound **3k**, produced

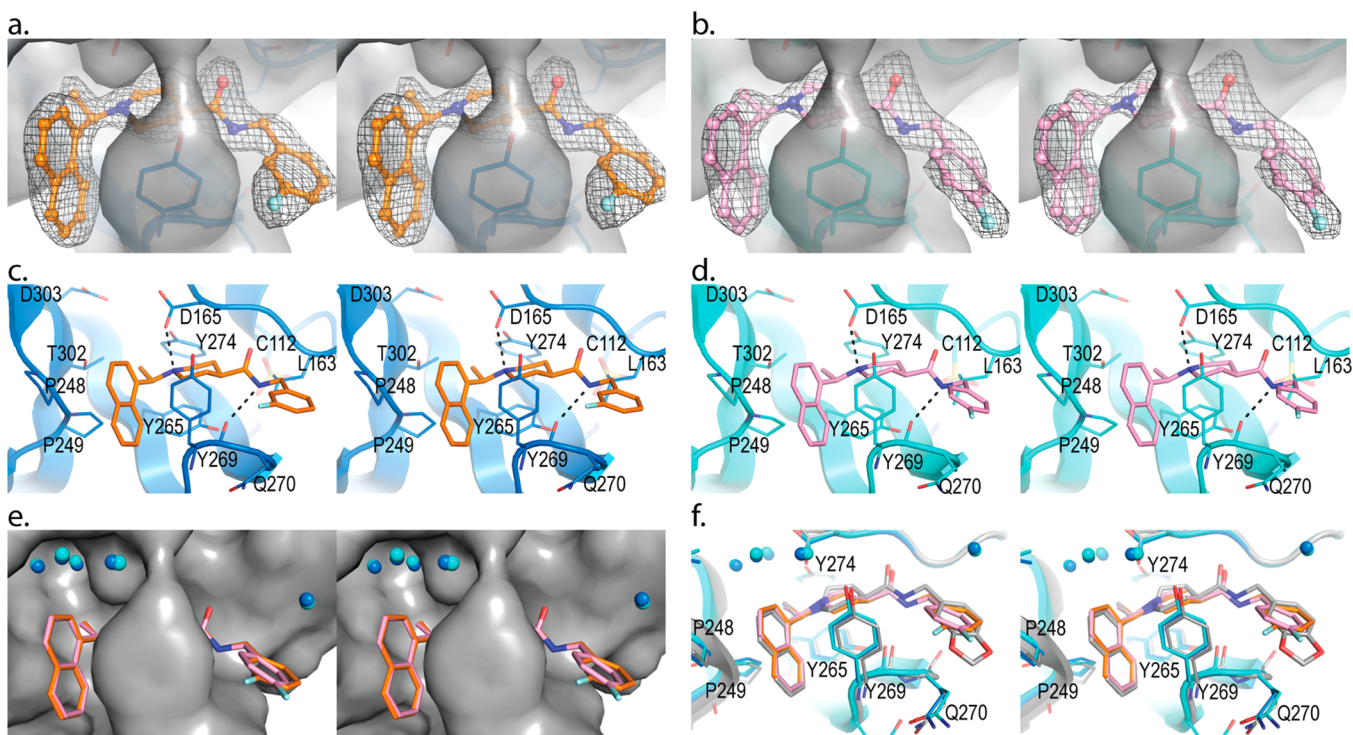


Figure 3. X-ray crystal structures of SARS-CoV PLpro in complex with **3k** and **3j**. Stereoviews of SARS-CoV PLpro (blue ribbon representation and gray surfaces) in complex with **3k** (orange ball and sticks) are shown in (a) and (c), and SARS-CoV PLpro (cyan ribbon representation and gray surface) in complex with **3j** (pink ball and sticks) are shown in (b) and (d). The corresponding $F_o - F_c$ electron density omit maps (inhibitor atoms omitted) contoured at 3σ are shown as gray mesh. Important amino acids for inhibitor binding are shown, and the H-bonds between inhibitor atoms and amino acid residues are depicted as dotted lines. A superimposition of SARS-CoV PLpro-**3k** and PLpro-**3j** complexes is shown in (e) with conserved water molecules displayed as blue and cyan spheres for the **3k**- and **3j**- complexes, respectively. A superimposition of SARS-CoV PLpro-**15g** complex (SARS-CoV PLpro displayed as a gray ribbon and **15g** displayed as gray balls and sticks, pdb:3MJ5) with SARS-CoV PLpro-**3k** and PLpro-**3j** complex is shown in (f).

Table 4. Inhibitor Selectivity against Human DUBs and Cysteine Proteases

	IC_{50} (μM) ^a			
	15g	3k	3e	3j
human DUB				
USP2	–	–	>100	–
USP7	–	–	>100	–
USP8	>100	>100	>100	>100
USP20	–	>100	>100	>100
USP21	>31	>31	>31	>31
DEN1	–	–	–	–
UCHL1	–	–	–	–
caspase 3	–	–	–	–
cathepsin K	–	–	–	–

^a–, no inhibition.

typical dose response curves, and the inhibition data were fit to determine the IC_{50} and maximum percent inhibition values (Table 5). The results show that inhibition of HCoV-NL63 PLP2 is achieved by this series of compounds, albeit significantly weaker inhibition than for SARS-CoV PLpro (micromolar versus nanomolar range), and suggest that SARS-CoV PLpro and HCoV-NL63 PLP2 may display sufficient structural similarities at the active site for the potential development of a dual-target inhibitor.

SARS-CoV Antiviral Activity and Cytotoxicity Evaluation of the Most Potent Compounds. Compound **3k** exhibits lower topological polar surface area (tPSA = 32.2 Å²)

Table 5. Compounds Displaying Dual-Target Inhibition of SARS-CoV PLpro and HCoV-NL63 PLP2

compd	IC_{50} (μM)		max I (%)	
	PLpro	PLP2	PLpro	PLP2
15g	0.67	18	99	46
3k	0.15	33	100	57
5c	0.35	59	100	67
3e	0.39	46	100	71
3d	5.7	37	94	42
3i	29	44	78	48

relative to the initial inhibitor **15g** (tPSA = 50.8 Å²) and therefore is proposed to enhance cell permeability and thus antiviral activity relative to **15g**. On the basis of these possible improvements, compound **3k** along with seven of the most potent analogues and two quinolone derivatives were subjected to antiviral assays using our well-established method and BSL-3 protocols.¹⁴ In this assay, compounds are titrated in both mock- and SARS-CoV-infected Vero E6 cells, and the resulting dose-response curves are fitted to the four-parameter logistic equation. Curves were then compared to the mock-infected cells to assess drug-induced cytotoxicity in Vero E6 and HEK293 cell lines. The resultant EC_{50} values and cytotoxic concentrations (CC_{50}) are shown in Table 6. Because of their greater potency, all tested compounds displayed low cytotoxicity levels ($CC_{50} > 68 \mu M$) with improved therapeutic index (TI) values in Vero E6 cell when compared to **15g**. Compounds with IC_{50} values of $>2 \mu M$ (**2a**, **4a**, and **4c**) had

Table 6. Compound Effect on Replication of SARS-CoV Virus, Cytotoxicity, and Therapeutic Indexes

	15g	3k	3e	5c	3j	2e
			Vero E6			
IC ₅₀ ^a	0.67 ± 0.03	0.15 ± 0.01	0.39 ± 0.01	0.35 ± 0.02	0.49 ± 0.01	1.9 ± 0.1
EC ₅₀ ^a	12.8 ± 1.4	5.4 ± 0.6	8.3 ± 0.6	9.5 ± 1.3	11.6 ± 0.8	11.7 ± 0.7
CC ₅₀ ^a	>100	>100	>100	>100	>100	>100
TI	>7.8	>18.5	>12	>10.5	>8.6	>8.5
			HEK293			
CC ₅₀ ^a	>100	73 ± 19	68 ± 15	>100	73 ± 29	>100

^aValues are reported in μM as mean \pm standard deviation based on a minimum of triplicate measurements. EC₅₀ values were derived from two independent experiments. EC₅₀, the half maximal effective concentration in SARS-CoV infected Vero E6 cells; CC₅₀, 50% cytotoxic concentration; TI, the therapeutic index defined as the ratio of CC₅₀/EC₅₀.

no antiviral activity displaying EC₅₀ values of $>50 \mu\text{M}$ (data not shown). Compounds **3e**, **5c**, **3j**, and **2e** displayed similar to slightly improved antiviral activity when compared to the initial compound **15g**. However, in the case of our best compound, **3k**, which has a 4-fold improved IC₅₀ value, an additional 2-fold improvement in antiviral activity was observed (EC₅₀ = $5.4 \pm 0.6 \mu\text{M}$) when compared to **15g**.

Metabolic Stability and Plasma Binding Studies. With the ultimate goal of achieving protection from coronavirus infection in vivo, we evaluated the stability of our best new analogues to phase I metabolism by mouse liver microsomes (Table 7). The lead compound **15g** proved to be exceedingly

Table 7. Stability of Selected Compounds to Metabolism by Mouse Liver Microsomes^a

compd	% rem (15 min) ^a	T _{1/2} (min) ^b
15g	0.2	1.6
3k	1.2	2.8
3e	20	7.0
5c	30	8.0

^aPercent of the parent compound remaining after 15 min incubation. The initial concentration of the parent compound was $1 \mu\text{M}$. ^bHalf-life (minutes) of parent compound.

unstable, being completely consumed within 15 min. This was not entirely unexpected because of the presence of the 3,4-methylenedioxy moiety, which renders the benzyl aromatic ring electron-rich and is itself a known target of cytochrome P450s.^{22,23} Somewhat surprisingly, the much more electron-poor 3-fluorobenzamide **3k** was still metabolized rapidly, suggesting that most of the metabolism is occurring distal to the benzamide. Consistent with this hypothesis, the less lipophilic bis(amide) **3e** and methoxypyridine **5c** were significantly more stable, with 20% and 30% parent drug remaining after 15 min, respectively, and half-lives 4- to 5-fold longer than that of **15g**.

Because the binding of an antiviral drug to human serum proteins may result in reduced antiviral activity,²⁴ we evaluated

the plasma binding ability of the compounds in Table 6 by measuring the shifts in their IC₅₀ values in various concentrations of human plasma protein (serum shift assays).²⁵ We observed no significant changes in the IC₅₀ values for the compounds in the serum shift assays, which were performed in the presence of 5%, 10%, and 20% human serum albumin (HSA) (data not shown), the most abundant protein in human plasma (40 mg/mL).²⁶ This observation suggests that no specific interactions between the compounds and HSA take place.

CONCLUSIONS

A second-generation series of highly potent SARS-CoV PLpro inhibitors was designed and evaluated biologically to further advance anticoronavirus drug development. Four compounds (**3k**, **3e**, **3j**, and **5c**) were found to have more potent SARS-CoV PLpro inhibition and SARS-CoV antiviral activity than the most potent first generation inhibitor, **15g**. None of these five compounds exhibit cytotoxicity or off-target inhibitory activity of a series of human DUB and cysteine protease enzymes, nor do any of these five inhibitors bind to human serum albumin (HSA). The second-generation compounds **3k**, **3e**, and **5c** exhibit significantly improved metabolic stability compared to **15g**. Although compound **3k** is the most potent SARS-CoV PLpro inhibitor (IC₅₀ = $0.15 \mu\text{M}$) and the most effective antiviral compound in cell culture (EC₅₀ = $5.4 \mu\text{M}$), it is significantly less metabolically stable compared to compounds **3e** and **5c**, which are similarly effective in inhibiting SARS-CoV PLpro (IC₅₀ = $0.39 \mu\text{M}$ and IC₅₀ = $0.35 \mu\text{M}$) and inhibiting SARS-CoV infected Vero cells (EC₅₀ = $8.3 \mu\text{M}$ and EC₅₀ = $9.5 \mu\text{M}$). Thus, compounds **3e** and **5c** are likely to be the better candidates to advance to animal efficacy models. Finally, the high resolution of the inhibitor-bound crystal structures of PLpro with **3k** and **3j** revealed novel aspects for the inhibitor binding mode, providing guidance for the further optimization of PLpro inhibitors.

■ EXPERIMENTAL SECTION

General Synthetic Procedures. All reagents were used as received from commercial sources unless otherwise noted. ^1H and ^{13}C spectra were obtained in DMSO- d_6 or CDCl_3 at room temperature, unless otherwise noted, on Varian Inova 400 MHz, Varian Inova 500 MHz, Bruker Avance DRX 500, or Bruker Avance DPX 300 instrument. Chemical shifts for the ^1H NMR and ^{13}C NMR spectra were recorded in parts per million (ppm) on the δ scale from an internal standard of residual tetramethylsilane (0 ppm). Rotamers are described as a ratio of rotamer A to rotamer B if possible. Otherwise, if the rotamers cannot be distinguished, the NMR peaks are described as multiplets. Mass spectrometry data were obtained on a Waters Corporation LCT. Purity of all tested compounds was assessed by HPLC using an Agilent 1100 series with an Agilent Zorbax Eclipse Plus C18 column (254 nm detection) with the following gradient: 10% ACN/water (1 min), 10–90% ACN/water (6 min), and 90% ACN/water (2 min). Values for each compound are included at the end of each experimental procedure, and all are over 95% pure. HPLC retention times (t_{R}) were recorded in minutes (min). Solvent abbreviations used are the following: MeOH (methanol), DCM (dichloromethane), EtOAc (ethyl acetate), Hex (hexanes), DMSO (dimethylsulfoxide), DMF (dimethylformamide), H_2O (water), THF (tetrahydrofuran), ACN (acetonitrile). Reagent abbreviations used are the following: HATU (*O*-(7-azabenzotriazol-1-yl)-*N,N,N',N'*-tetramethyluronium hexafluorophosphate), HOAT (1-hydroxy-7-azabenzotriazole), HOBt (1-hydroxy-1,2,3-benzotriazole), EDCI (*N*-(3-dimethylaminopropyl)-*N'*-ethylcarbodiimide hydrochloride), DIEA (diisopropylethylamine), TFA (trifluoroacetic acid), MgSO_4 (magnesium sulfate), Na_2SO_4 (sodium sulfate), NaHCO_3 (sodium bicarbonate), Na_2CO_3 (sodium carbonate), Cs_2CO_3 (cesium carbonate), NH_4Cl (ammonium chloride), K_2CO_3 (potassium carbonate), KOH (potassium hydroxide), HCl (hydrogen chloride), NaOH (sodium hydroxide), LiOH (lithium hydroxide), LAH (lithium aluminum hydride), EtOH (ethanol), NaCN (sodium cyanide), Et_2O (diethyl ether), CsF (cesium fluoride), NaCl (sodium chloride), TBSCl (*tert*-butyldimethylsilyl chloride), Ms_2O (methanesulfonic anhydride), MsCl (methanesulfonyl chloride), AcOH (acetic acid), NaBH_4 (sodium borohydride), NaBH_3CN (sodium cyanoborohydride), H_2 (hydrogen), N_2 (nitrogen), MS (molecular sieves). Assay abbreviations are the following: LUC (luciferase), MTT ((3-(4,5-dimethylthiazol-2-yl)-2,5-diphenyltetrazolium bromide. Additional abbreviations are the following: aq (aqueous), saturated (saturated), rt (room temperature). All anhydrous reactions were run under an atmosphere of dry nitrogen.

(±)-*N*-(Benzo[*d*][1,3]dioxol-5-ylmethyl)-1-(1-(naphthalen-1-yl)propyl)piperidine-4-carboxamide (1a). Ethyl 1-(1-(naphthalen-1-yl)propyl)piperidine-4-carboxylate **11a** (480 mg, 1.48 mmol) was dissolved in a 1:1:2 mixture of THF/EtOH/1 M aqueous NaOH, total volume of 8 mL. This was stirred at 60 °C for 5 h. The mixture was allowed to cool, and the organic solvents in the mixture were mostly removed by rotary evaporation. The pH was then reduced by addition of concentrated HCl to ~pH 4, and the resulting white precipitate was collected over a filter to give the desired carboxylic acid (364 mg, 83%) without further purification. Then the following was added sequentially to anhydrous DMF (1 mL): 3 Å molecular sieves, 1-(1-(naphthalen-1-yl)propyl)piperidine-4-carboxylic acid (50 mg, 0.17 mmol), DIEA (0.088 mL, 0.504 mmol), EDCI (36 mg, 0.19 mmol), HOBt (28 mg, 0.19 mmol), and finally piperonylamine (0.031 mL, 0.252 mmol). This was stirred at room temperature for 16 h, at which time the material was partitioned between 10% Na_2CO_3 solution and EtOAc, and the organic layer was washed with 10% Na_2CO_3 solution (3 × 20 mL) and brine (1 × 20 mL). The organic layer was dried with anhydrous MgSO_4 , filtered, and concentrated in vacuo. Purification was accomplished via flash chromatography (4 g silica RediSep gold column on a CombiFlash, eluted with 70% EtOAc/Hex) to give the desired product (34 mg, 47%). ^1H NMR (500 MHz, chloroform-*d*) δ 8.44 (bs, 1H), 7.91–7.84 (m, 1H), 7.77 (d, *J* = 8.1 Hz, 1H), 7.53–7.40 (m, 4H), 6.78–6.66 (m, 3H), 5.94 (s, 2H), 5.87–5.81 (m, 1H), 4.32 (d, *J* = 5.6 Hz, 2H), 3.93 (bs, 1H), 3.39–3.26 (m,

1H), 2.94–2.80 (m, 1H), 2.25 (bs, 1H), 2.06–1.66 (m, 8H), 0.68 (t, *J* = 7.1 Hz, 3H). TOF ES+ MS: (M + H) 431.1. HPLC t_{R} = 5.85 min, >95% purity.

(±)-*N*-(Benzo[*d*][1,3]dioxol-5-ylmethyl)-1-(2-hydroxy-1-(naphthalen-1-yl)ethyl)piperidine-4-carboxamide (1b). Silyl ether **17** (46 mg, 0.08 mmol) was dissolved in ACN (4 mL) and H_2O (2 mL). To this was added CsF (51 mg, 0.34 mmol), and the mixture was stirred at room temperature for 24 h. The mixture was then partitioned between 10% aqueous Na_2CO_3 (30 mL) and EtOAc (50 mL) and extracted. The extract was dried with anhydrous MgSO_4 , filtered, and concentrated in vacuo. The residue was then purified by flash chromatography (4.7g amine-activated silica RediSep column, 50% EtOAc/Hex) to give the final product (28 mg, 77%). ^1H NMR (500 MHz, chloroform-*d*) δ 8.29 (d, *J* = 8.2 Hz, 1H), 7.90 (d, *J* = 8.0 Hz, 1H), 7.87–7.81 (m, 1H), 7.58–7.45 (m, 4H), 6.81–6.64 (m, 3H), 5.95 (s, 2H), 5.69 (t, *J* = 4.7 Hz, 1H), 4.64–4.49 (m, 1H), 4.32 (d, *J* = 5.6 Hz, 2H), 4.09 (dd, *J* = 11.0, 7.8 Hz, 1H), 3.81 (dd, *J* = 10.9, 5.2 Hz, 1H), 3.27 (d, *J* = 11.2 Hz, 1H), 3.00 (d, *J* = 11.5 Hz, 1H), 2.32–1.75 (m, 7H). TOF ES+ MS: (M + H) 433.1, (M + Na) 455.1. HPLC t_{R} = 5.43 min, >95% purity.

(±)-*N*-(Benzo[*d*][1,3]dioxol-5-ylmethyl)-1-(2-methoxy-1-(naphthalen-1-yl)ethyl)piperidine-4-carboxamide (1c). Ethyl 1-(2-methoxy-1-(naphthalen-1-yl)ethyl)piperidine-4-carboxylate **11c** (80 mg, 0.23 mmol) was dissolved in EtOH (2 mL) and 6 M NaOH (5 mL). This was stirred at 50 °C for 3 h. The pH was dropped to 2 by dropwise addition of concentrated HCl, and material was extracted with 1:1 EtOAc/ Et_2O (3 × 10 mL). The solvent was then dried with anhydrous MgSO_4 , filtered, and removed in vacuo to give 1-(2-methoxy-1-(naphthalen-1-yl)ethyl)piperidine-4-carboxylic acid (30 mg, 41%) without further purification. Then the following was added sequentially to anhydrous DMF (1 mL): 3 Å molecular sieves, 1-(2-methoxy-1-(naphthalen-1-yl)ethyl)piperidine-4-carboxylic acid (20 mg, 0.06 mmol), DIEA (0.033 mL, 0.191 mmol), EDCI (14 mg, 0.07 mmol), HOBt (11 mg, 0.07 mmol), and finally piperonylamine (0.012 mL, 0.096 mmol). This was stirred at room temperature for 24 h, at which time the material was partitioned between 10% aqueous Na_2CO_3 solution and EtOAc, and the organic layer was washed with 10% aqueous Na_2CO_3 solution (3 × 10 mL) and brine (1 × 10 mL). The organic layer was dried with anhydrous MgSO_4 , filtered, and concentrated in vacuo. The material was purified via alumina flash chromatography (8 g basic alumina RediSep cartridge, 30% EtOAc/Hex) to give the final desired compound (13 mg, 46%). ^1H NMR (500 MHz, chloroform-*d*) δ 8.37 (d, *J* = 7.8 Hz, 1H), 7.88 (d, *J* = 7.2 Hz, 1H), 7.78 (d, *J* = 8.1 Hz, 1H), 7.60 (d, *J* = 7.0 Hz, 1H), 7.54–7.47 (m, 2H), 7.45 (t, *J* = 7.6 Hz, 1H), 6.79–6.71 (m, 3H), 5.96 (s, 2H), 5.73 (s, 1H), 4.34 (d, *J* = 5.6 Hz, 2H), 4.21 (s, 1H), 3.93 (dd, *J* = 10.1, 6.3 Hz, 1H), 3.67 (dd, *J* = 10.3, 3.5 Hz, 1H), 3.36 (d, *J* = 11.1 Hz, 1H), 3.31 (s, 3H), 2.85 (d, *J* = 11.4 Hz, 1H), 2.24 (t, *J* = 10.8 Hz, 1H), 2.16–2.09 (m, 1H), 2.07–1.69 (m, 5H). TOF ES+ MS: (M + H) 447.1, (M + Na) 469.1. HPLC t_{R} = 5.97 min, >95% purity.

(±)-*N*-(Benzo[*d*][1,3]dioxol-5-ylmethyl)-1-(1-(naphthalen-1-yl)-2-phenylethyl)piperidine-4-carboxamide (1d). Methyl 1-(1-(naphthalen-1-yl)-2-phenylethyl)piperidine-4-carboxylate **23** (38 mg, 0.10 mmol) was dissolved in a 1:1:2 mixture of THF/EtOH/1 M aqueous NaOH, total volume of 4 mL. This was stirred at 60 °C for 4 h. The mixture was allowed to cool, and the pH was reduced by addition of concentrated HCl to ~pH 4, and the resulting white precipitate was collected over a filter to give 1-(1-(naphthalen-1-yl)-2-phenylethyl)piperidine-4-carboxylic acid (30 mg, 82%) as a white powder. Then the following was added sequentially to anhydrous DMF (1 mL): 3 Å molecular sieves, 1-(1-(naphthalen-1-yl)-2-phenylethyl)piperidine-4-carboxylic acid (30 mg, 0.08 mmol), DIEA (44 μL , 0.25 mmol), EDCI (18 mg, 0.09 mmol), HOBt (14 mg, 0.09 mmol), and piperonylamine (16 μL , 0.13 mmol). This was stirred at room temperature for 17 h, at which time the material was partitioned between 10% aqueous Na_2CO_3 solution and EtOAc, and the organic layer was washed with 10% aqueous Na_2CO_3 solution (3 × 20 mL) and brine (1 × 20 mL). The organic layer was dried with anhydrous MgSO_4 , filtered, and concentrated in vacuo. The residue was then purified by flash chromatography (10 g silica, 50% EtOAc/Hex) to

give the final product (20 mg, 44%). ¹H NMR (500 MHz, chloroform-*d*) δ 8.47 (bs, 1H), 7.86–7.80 (m, 1H), 7.72 (d, *J* = 8.8 Hz, 1H), 7.46 (dt, *J* = 6.3, 3.3 Hz, 2H), 7.31 (bs, 2H), 7.12–7.00 (m, 3H), 6.89 (bs, 2H), 6.77–6.70 (m, 3H), 5.95 (s, 2H), 5.83–5.74 (m, 1H), 4.33 (d, *J* = 5.7 Hz, 2H), 3.46 (dd, *J* = 13.6, 4.8 Hz, 1H), 3.41 (s, 1H), 3.20 (dd, *J* = 13.6, 9.1 Hz, 1H), 2.95 (d, *J* = 9.8 Hz, 1H), 2.15–2.04 (m, 3H), 1.91–1.70 (m, 4H). TOF ES+ MS: (M + H) 493.1, (M + Na) 515.1. HPLC *t*_R = 6.22 min, >95% purity.

General Amide Coupling Method A. To a solution of HOAT (0.07 g, 0.35 mmol) in dry DMF (5 mL) were added HATU (0.19 g, 0.49 mmol), (*R*)-1-(1-(naphthalen-1-yl)ethyl)piperidine-4-carboxylic acid **25** (0.1 g, 0.35 mmol), and amine (0.42 mmol) followed by DIEA (0.05 g, 0.35 mmol). The mixture was stirred overnight at room temperature, then diluted with saturated aqueous NaHCO₃ and extracted with EtOAc (3×). The combined organic extracts were washed with saturated NaCl (3×), dried (MgSO₄), and concentrated. The residue was purified by silica gel flash chromatography (1–4% MeOH/DCM).

General Amide Coupling Method B. To a solution of (*R*)-1-(1-(naphthalen-1-yl)ethyl)piperidine-4-carboxylic acid **25** (0.06 g, 0.21 mmol) in dry DMF (5 mL) were added EDCI (0.05 g, 0.28 mmol), HOBt (0.04 g, 0.25 mmol), and DIEA (0.07 mL, 0.53 mmol), followed by amine (0.21 mmol) and stirred overnight at room temperature. After this time, the reaction mixture was diluted with saturated NaHCO₃ and extracted with EtOAc (3×). The combined organic extracts were washed with saturated NaCl (3×), dried (MgSO₄), and concentrated. The residue was purified by silica gel flash chromatography (1–5% MeOH/DCM).

(*R*)-*N*-Benzyl-1-(1-(naphthalen-1-yl)ethyl)piperidine-4-carboxamide (2a). Coupling method A: 42% yield. ¹H NMR (400 MHz, DMSO-*d*₆) δ 8.44 (br s, 1H), 7.80–7.90 (m, 1H), 7.75–7.79 (m, 1H), 7.23–7.61 (m, 10H), 5.88 (s, 1H), 5.45 (br s, 1H), 4.32 (m, 2H), 4.20 (br s, 1H), 3.23–3.34 (m, 1H), 2.88–2.91 (m, 2H), 1.84–2.03 (m, 4H), 1.43 (m, 3H). TOF ES+ MS: (M + H) 373.2. HPLC *t*_R = 5.8 min, >95% purity.

1-((*R*)-1-(Naphthalen-1-yl)ethyl)-*N*-((*R*)-1-phenylethyl)piperidine-4-carboxamide (2b). Coupling method A: 33% yield. ¹H NMR (400 MHz, DMSO-*d*₆) δ 8.44 (d, *J* = 4.7 Hz, 1H), 7.86–7.88 (m, 1H), 7.76 (d, *J* = 6.48 Hz, 1H), 7.56 (br s, 1H), 7.42–7.48 (m, 3H), 7.32–7.34 (m, 5H), 5.68 (br s, 1H), 5.13–5.16 (m, 1H), 4.13 (br s, 1H), 3.25 (d, *J* = 8.5 Hz, 1H), 2.29 (d, *J* = 6.4 Hz, 1H), 2.02–2.10 (m, 2H), 1.89–1.91 (m, 1H), 1.67–1.79 (m, 4H), 1.46–1.48 (m, 3H). TOF ES+ MS: (M + H) 387.2. HPLC *t*_R = 5.9 min, >95% purity.

1-((*R*)-1-(Naphthalen-1-yl)ethyl)-*N*-((*S*)-1-phenylethyl)piperidine-4-carboxamide (2c). Coupling method A: 23% yield. ¹H NMR (400 MHz, DMSO-*d*₆ and CDCl₃) δ 8.22 (m, 1H), 7.86–8.1 (m, 2H), 7.72–7.81 (m, 2H), 7.32–7.48 (m, 4H), 7.32–7.38 (m, 3H), 6.96 (br s, 1H), 5.11 (br s, 1H), 4.89–4.91 (m, 1H), 5.13–5.16 (m, 1H), 4.65–4.4.69 (m, 1H), 3.72–3.79 (m, 2H), 3.68–3.72 (m, 1H), 3.68–3.65 (m, 1H), 2.29 (m, 1H), 2.02–2.12 (m, 1H), 1.89–1.91 (m, 1H), 1.62–1.74 (m, 3H), 1.46–1.48 (m, 3H). TOF ES+ MS: (M + H) 387.2. HPLC *t*_R = 5.9 min, >95% purity.

***N*-((*R*)-2-Methoxy-1-phenylethyl)-1-((*R*)-1-(naphthalen-1-yl)ethyl)piperidine-4-carboxamide (2d).** Coupling method B: 60% yield. ¹H NMR (400 MHz, chloroform-*d*) δ 8.43 (d, *J* = 8.0 Hz, 1H), 7.82–7.85 (m, 1H), 7.73 (m, 1H), 7.56 (d, *J* = 7.2 Hz, 1H), 7.43–7.46 (m, 2H), 7.24–7.46 (m, 5H), 6.17 (d, *J* = 7.6 Hz, 1H), 5.15 (d, *J* = 7.2 Hz, 1H), 4.09–4.11 (m, 1H), 3.63 (d, *J* = 4.7 Hz, 2H), 3.31 (s, 3H), 3.23 (d, *J* = 11.3 Hz, 1H), 2.89 (d, *J* = 11.4 Hz, 1H), 1.99–2.27 (m, 3H), 1.57–1.95 (m, 4H), 1.47 (d, *J* = 6.7 Hz, 2H). TOF ES+ MS: (M + H) 417.2. HPLC *t*_R = 5.6 min, >95% purity.

***N*-((*S*)-2-Methoxy-1-phenylethyl)-1-((*R*)-1-(naphthalen-1-yl)ethyl)piperidine-4-carboxamide (2e).** Coupling method B: 52% yield. ¹H NMR (400 MHz, chloroform-*d*) δ 8.43 (d, *J* = 8.0 Hz, 1H), 7.82–7.84 (m, 1H), 7.72 (d, *J* = 8.2 Hz, 1H), 7.56 (d, *J* = 7.2 Hz, 1H), 7.35–7.52 (m, 2H), 6.99–7.35 (m, 5H), 6.12 (d, *J* = 7.7 Hz, 1H), 5.14 (d, *J* = 7.1 Hz, 1H), 4.10 (m, 1H), 3.63 (d, *J* = 4.7 Hz, 2H), 3.32 (s, 3H), 3.22 (d, *J* = 11.3 Hz, 1H), 2.88 (d, *J* = 11.6 Hz, 1H), 1.99–2.28 (m, 3H), 1.95–1.50 (m, 4H), 1.46 (d, *J* = 6.7 Hz, 2H). TOF ES+ MS: (M + H) 417.2. HPLC *t*_R = 5.6 min, >95% purity.

(*R*)-*N*-(4-Ethylbenzyl)-1-(1-(naphthalen-1-yl)ethyl)piperidine-4-carboxamide (3a). Coupling method B: 26% yield. ¹H NMR (400 MHz, chloroform-*d*) δ 8.41 (d, *J* = 7.9 Hz, 1H), 7.82–7.83 (m, 1H), 7.71–7.73 (m, 1H), 7.39–7.45 (m, 4H), 7.12–7.16 (m, 4H), 5.68 (m, 1H), 4.37 (d, *J* = 5.5 Hz, 2H), 3.99–4.20 (m, 1H), 3.22 (d, *J* = 11.2 Hz, 1H), 2.87 (d, *J* = 11.2 Hz, 1H), 2.61 (q, *J* = 7.6 Hz, 2H), 1.91–2.24 (m, 4H), 1.57–1.81 (m, 3H), 1.45 (d, *J* = 6.7 Hz, 3H), 1.20 (td, *J* = 7.6, 0.6 Hz, 3H). TOF ES+ MS: (M + H) 401.1. HPLC *t*_R = 5.9 min, 94% purity.

(*R*)-*N*-(4-(Methylcarbamoyl)benzyl)-1-(1-(naphthalen-1-yl)ethyl)piperidine-4-carboxamide (3b). Coupling method B: 50% yield. ¹H NMR (400 MHz, chloroform-*d*) δ 8.38 (s, 1H), 7.76–7.99 (m, 1H), 7.73 (d, *J* = 8.2 Hz, 1H), 7.59–7.70 (m, 2H), 7.53–7.32 (m, 4H), 7.20–7.32 (m, 2H), 6.20 (s, 2H), 4.42 (d, *J* = 6.0 Hz, 2H), 4.16 (d, *J* = 16.5 Hz, 1H), 3.22 (d, *J* = 10.8 Hz, 1H), 2.93–3.09 (m, 2H), 2.91 (d, *J* = 7.4 Hz, 1H), 1.32–2.28 (m, 9H). TOF ES+ MS: (M + H) 430.2. HPLC *t*_R = 4.7 min, >95% purity.

(*R*)-*N*-(3-(Methylcarbamoyl)benzyl)-1-(1-(naphthalen-1-yl)ethyl)piperidine-4-carboxamide (3c). To a solution of *tert*-butyl 3-(methylcarbamoyl)benzoic acid (0.3 g, 1.1 mmol) in dry DMF (15 mL) were added EDCI (0.26 g, 1.36 mmol), HOBt (0.21 g, 1.36 mmol), and DIEA (0.39 mL, 2.27 mmol), followed by methanamine (0.03 g, 1.10 mmol). The mixture was stirred overnight at room temperature. After dilution with saturated aqueous NaHCO₃, the aqueous layer was extracted with EtOAc (2×). The combined organic layers were washed with saturated NaCl (3×) and dried (MgSO₄), concentrated in vacuo, and purified by flash chromatography (1–4% MeOH/DCM) to provide the intermediate (0.1g, 54%). ¹H NMR (400 MHz, chloroform-*d*) δ 8.01 (s, 1H), 7.61–7.69 (m, 2H), 7.28–7.41 (m, 3H), 4.32 (br s, 2H), 2.99 (d, *J* = 4.3 Hz, 3H), 1.49 (s, 9H). TOF ES+ MS: (M + H) 165.1. This material was treated with 4 M HCl in dioxane and stirred overnight at room temperature. After being concentrated in vacuo, the crude 3-(aminomethyl)-*N*-methylbenzamide was coupled with **25** using method B to afford the desired compound (0.02 g, 11%). ¹H NMR (400 MHz, chloroform-*d*) δ 8.40 (s, 1H), 7.84 (d, *J* = 7.5 Hz, 1H), 7.73 (d, *J* = 8.1 Hz, 1H), 7.63 (d, *J* = 13.5 Hz, 2H), 7.37–7.54 (m, 2H), 7.35 (d, *J* = 4.6 Hz, 1H), 6.20 (m, 1H), 5.87 (m, 1H), 4.44 (d, *J* = 5.8 Hz, 2H), 4.11 (d, *J* = 7.2 Hz, 1H), 3.23 (s, 1H), 2.99 (d, *J* = 4.8 Hz, 2H), 2.91 (s, 1H), 0.75–2.24 (m, 13H). TOF ES+ MS: (M + H) 430.3. HPLC *t*_R = 4.8 min, 92% purity.

(*R*)-*N*-(4-Acetamidobenzyl)-1-(1-(naphthalen-1-yl)ethyl)piperidine-4-carboxamide (3d). Coupling method B: 23% yield. ¹H NMR (400 MHz, chloroform-*d*) δ 8.42 (d, *J* = 8.0 Hz, 1H), 7.76–7.89 (m, 3H), 7.72 (d, *J* = 8.1 Hz, 1H), 7.55 (d, *J* = 7.2 Hz, 1H), 7.33–7.49 (m, 5H), 6.22 (m, 1H), 5.83 (m, 1H), 4.08 (q, *J* = 6.5 Hz, 1H), 3.64 (s, 3H), 3.12 (d, *J* = 11.4 Hz, 1H), 2.81 (d, *J* = 11.3 Hz, 1H), 2.13–2.40 (m, 1H), 1.95–2.15 (m, 2H), 1.84–1.97 (m, 1H), 1.64–1.84 (m, 3H), 1.45 (d, *J* = 6.7 Hz, 3H). TOF ES+ MS: (M + H) 430.3. HPLC *t*_R = 5.19 min, >95% purity.

(*R*)-*N*-(3-Acetamidobenzyl)-1-(1-(naphthalen-1-yl)ethyl)piperidine-4-carboxamide (3e). Coupling method B: 90% yield. ¹H NMR (400 MHz, chloroform-*d*) δ 8.41 (d, *J* = 7.8 Hz, 1H), 7.78–7.93 (m, 1H), 7.72 (d, *J* = 8.2 Hz, 1H), 7.30–7.64 (m, 5H), 7.23 (d, *J* = 6.6 Hz, 2H), 6.95 (d, *J* = 7.6 Hz, 1H), 5.80 (s, 1H), 4.36 (d, *J* = 5.7 Hz, 2H), 3.90–4.25 (m, 2H), 3.21 (d, *J* = 11.1 Hz, 1H), 2.87 (d, *J* = 11.1 Hz, 1H), 1.94–2.24 (m, 5H), 1.53–1.94 (m, 2H), 1.45 (d, *J* = 6.6 Hz, 3H), 1.24 (td, *J* = 7.1, 0.6 Hz, 2H). TOF ES+ MS: (M + H) 430.1. HPLC *t*_R = 5.0 min, >95% purity.

(*R*)-*N*-(3-(Acetamidomethyl)benzyl)-1-(1-(naphthalen-1-yl)ethyl)piperidine-4-carboxamide (3f). To a solution of 1,3-phenylenedimethanamine (0.2 g, 1.4 mmol) in THF (20 mL) was added acetic anhydride (0.07 mL, 0.73 mmol) in THF (10 mL) dropwise. The resulting mixture was stirred overnight at room temperature, then concentrated, and the residue was purified by silica gel flash chromatography (1–5% MeOH/DCM), providing *N*-(3-(aminomethyl)benzyl)acetamide (0.06 g, 23% yield, TOF ES+ MS, (M + H) 178.1) which was subsequently coupled with **25** using method B to afford the final compound (0.02 g, 12%). ¹H NMR (400 MHz, chloroform-*d*) δ 8.42 (d, *J* = 7.4 Hz, 1H), 7.76–7.94 (m, 1H), 7.73 (m, 1H), 7.49–7.62 (m, 5H), 7.32–7.48 (m, 3H), 4.08 (m, 2H),

3.64 (s, 3H), 3.12 (d, $J = 12.2$ Hz, 1H), 2.80 (d, $J = 12.2$ Hz, 1H), 2.23–2.27 (m, 1H), 1.91–2.06 (m, 2H), 1.64–1.81 (m, 6H), 1.44 (dd, $J = 6.7, 3.7$ Hz, 3H). TOF ES+ MS: (M + H) 444.3. HPLC $t_R = 5.4$ min, 94% purity.

(R)-N-(3-Chlorobenzyl)-1-(1-(naphthalen-1-yl)ethyl)piperidine-4-carboxamide (3g). Coupling method A: 22% yield. ^1H NMR (400 MHz, chloroform- d) δ 7.79–7.81 (m, 2H), 7.70 (s, 1H), 7.23–7.26 (m, 5H), 7.32–7.54 (m, 2H), 7.11–7.13 (m, 1H), 5.81 (br s, 1H), 4.40 (d, $J = 5.8$ Hz, 2H), 3.86 (s, 1H), 3.57–3.61 (m, 1H), 2.90–2.95 (m, 1H), 2.28–1.93 (m, 6H), 1.45 (d, $J = 6.7$ Hz, 3H). TOF ES+ MS: (M + H) 407.2. HPLC $t_R = 4.3$ min, >95% purity.

(R)-N-(4-Chlorobenzyl)-1-(1-(naphthalen-1-yl)ethyl)piperidine-4-carboxamide (3h). Coupling method B: 29% yield. ^1H NMR (400 MHz, chloroform- d) δ 8.39 (s, 1H), 7.79–7.96 (m, 1H), 7.73 (d, $J = 8.2$ Hz, 1H), 7.32–7.66 (m, 5H), 7.19–7.32 (m, 2H), 7.01–7.19 (m, 2H), 5.73 (br s, 1H), 4.36 (d, $J = 5.9$ Hz, 2H), 4.11 (br s, 1H), 3.22 (d, $J = 10.9$, 1H), 2.89 (br s, 1H), 1.73–2.09 (m, 6H), 1.47 (s, 3H). TOF ES+ MS: (M + H) 407.1. HPLC $t_R = 5.7$ min, >95% purity.

(R)-N-(3,4-Difluorobenzyl)-1-(1-(naphthalen-1-yl)ethyl)piperidine-4-carboxamide (3i). Coupling method A: 31% yield. ^1H NMR (400 MHz, chloroform- d) δ 7.79–7.81 (m, 3H), 7.70 (s, 1H), 7.43–7.51 (m, 3H), 7.03–7.12 (m, 2H), 6.96 (br s, 1H), 5.83 (br s, 1H), 4.37 (d, $J = 8.0$ Hz, 2H), 3.59–3.64 (m, 1H), 3.32–3.39 (m, 1H), 2.91–2.94 (m, 1H), 1.93–2.28 (m, 3H), 1.75–1.89 (m, 4H), 1.43 (d, $J = 6.7$ Hz, 3H). TOF ES+ MS: (M + H) 409.2. HPLC $t_R = 5.78$ min, >95% purity.

(R)-N-(4-Fluorobenzyl)-1-(1-(naphthalen-1-yl)ethyl)piperidine-4-carboxamide (3j). Coupling method B: 38% yield. ^1H NMR (400 MHz, chloroform- d) δ 8.42–8.44 (m, 1H), 7.85–7.87 (m, 1H), 7.73–7.74 (d, $J = 8.2$ Hz, 1H), 7.55–7.56 (m, 1H), 7.46–7.54 (m, 3H), 7.20–7.22 (m, 3H), 7.01–7.11 (m, 2H), 5.73 (s, 1H), 4.38–4.39 (d, $J = 4.8$ Hz, 2H), 4.09–4.11 (m, 1H), 3.22 (d, $J = 8.8$ Hz, 1H), 2.89 (d, $J = 9.2$ Hz, 1H), 1.91–2.06 (m, 3H), 1.71–1.84 (m, 3H), 1.47 (d, $J = 5.3$ Hz, 3H). TOF ES+ MS: (M + H) 391.2. HPLC $t_R = 5.9$ min, >95% purity.

(R)-N-(3-Fluorobenzyl)-1-(1-(naphthalen-1-yl)ethyl)piperidine-4-carboxamide (3k). Coupling method B: 12% yield. ^1H NMR (400 MHz, chloroform- d) δ 8.43 (s, 1H), 7.84–7.85 (m, 1H), 7.73 (d, $J = 6.5$ Hz, 1H), 7.56–7.57 (m, 1H), 7.41–7.48 (m, 2H), 7.21–7.27 (m, 1H), 7.02–7.06 (m, 1H), 6.93–6.95 (m, 1H), 5.75 (s, 1H), 4.42 (d, $J = 4.6$ Hz, 2H), 4.12 (br s, 1H), 3.24 (d, $J = 7.8$, 1H), 2.90 (d, $J = 9.7$, 1H), 1.99–2.14 (m, 2H), 1.90–1.93 (m, 1H), 1.57–1.80 (m, 5H), 1.46 (s, 3H). TOF ES+ MS: (M + H) 391.2. HPLC $t_R = 5.7$ min, >95% purity.

N-(3-Fluorobenzyl)-1-(1-(quinolin-8-yl)ethyl)piperidine-4-carboxylate (28a). Ethyl 1-(1-(quinolin-8-yl)ethyl)piperidine-4-carboxylate (0.38 g, 1.30 mmol) was dissolved in methanol (20 mL), followed by the addition of 1 N sodium hydroxide (2.6 mL, 2.6 mmol) in one portion. The resulting mixture was stirred for 18 h at room temperature, then concentrated in vacuo and partitioned between ether and a minimum amount of water. The layers were separated, and the aqueous layer was treated with AcOH dropwise until the solution was acidic by pH paper. The solution was then concentrated in vacuo and dried under high vacuum overnight at room temperature, and the resulting acid was used without further purification. To a solution of (*R,S*)-1-(1-(quinolin-8-yl)ethyl)piperidine-4-carboxylic acid (0.1 g, 0.35 mmol) in dry DMF (5 mL) was added EDCI (0.07 g, 0.35 mmol), HOBt (0.07 g, 0.42 mmol), and DIEA (0.06 mL, 0.35 mmol) followed by (3-fluorophenyl)methanamine (0.04 g, 0.35 mmol). This reaction mixture was stirred overnight at room temperature, after which it was diluted with saturated NaHCO_3 and extracted with EtOAc (1 \times). The combined organic layers were washed with saturated NaCl (3 \times) and dried (MgSO_4), then concentrated and purified by silica flash chromatography (1–5% MeOH/DCM) to obtain 4a (0.05 g, 33% yield). ^1H NMR (400 MHz, DMSO- d_6) δ 8.75–8.98 (m, 2H), 8.35 (m, 1H), 8.27 (t, $J = 6.0$ Hz, 1H), 7.87 (d, $J = 8.4$ Hz, 1H), 7.60–7.72 (m, 1H), 7.42–7.59 (m, 2H), 7.21–7.42 (m, 2H), 7.00 (ddd, $J = 23.3, 16.7, 9.5$ Hz, 2H), 3.84–4.40 (m, 4H), 2.94 (d, $J = 10.8$ Hz, 1H), 2.76 (d, $J = 10.8$ Hz, 1H), 1.88–2.30 (m, 2H), 1.39–1.76 (m, 2H), 1.37 (d, $J = 6.6$

Hz, 3H). TOF ES+ MS: (M + H) 392.2. HPLC $t_R = 4.1$ min, >95% purity.

N-(3-Fluorobenzyl)-1-(1-(quinolin-5-yl)ethyl)piperidine-4-carboxamide (4b). Ethyl 1-(1-(quinolin-5-yl)ethyl)piperidine-4-carboxylate 28b (0.67 g, 2.15 mmol) was dissolved in methanol (20 mL), followed by 1 N sodium hydroxide (4.29 mL, 4.29 mmol) in one portion. The resulting mixture was stirred 18 h at room temperature, concentrated in vacuo, and partitioned between ether and a minimum amount of water. The layers were separated, and the aqueous layer was treated with AcOH dropwise until the solution measured acidic by pH paper. The solution was concentrated in vacuo, dried under high vacuum, and the resulting carboxylic acid was used without further purification in the next step. To a solution of (*R,S*)-1-(1-(quinolin-5-yl)ethyl)piperidine-4-carboxylic acid (0.100 g, 0.352 mmol) in dry DMF (5 mL) were added EDCI (0.067 g, 0.350 mmol), HOBt (0.060 g, 0.420 mmol), and DIEA (0.060 mL, 0.35 mmol) followed by (3-fluorophenyl)methanamine (0.040 g, 0.350 mmol). The mixture was stirred overnight at room temperature, diluted with saturated NaHCO_3 , and extracted with EtOAc. The combined organic layers were washed with saturated NaCl (3 \times) and dried (MgSO_4), then concentrated and purified by silica gel flash chromatography (1–5% MeOH/DCM) to provide the target compound (0.05 g, 33%) as a colorless oil. ^1H NMR (400 MHz, chloroform- d) δ 8.84–8.89 (m, 1H), 7.96 (d, $J = 8.4$ Hz, 1H), 7.42–7.76 (m, 2H), 7.35 (dd, $J = 8.6, 4.2$ Hz, 1H), 7.13–7.32 (m, 2H), 6.74–7.07 (m, 3H), 6.02–5.97 (s, 1H), 4.15–4.39 (q, $J = 6.1$ Hz, 2H), 4.02 (q, $J = 6.7$ Hz, 1H), 2.96–3.23 (m, 1H), 2.65–2.96 (m, 1H), 1.94–2.17 (m, 6H), 1.54–1.88 (m, 4H), 1.44 (d, $J = 6.7$ Hz, 3H). TOF ES+ MS: (M + H) 392.1. HPLC $t_R = 3.9$ min, >95% purity.

N-(3-Fluorobenzyl)-1-(1-(isoquinolin-5-yl)ethyl)piperidine-4-carboxamide (4c). Ethyl 1-(1-(isoquinolin-5-yl)ethyl)piperidine-4-carboxylate 28c (0.50 g, 1.61 mmol) was dissolved in methanol (20 mL), followed by 1 N sodium hydroxide (3.2 mL, 3.2 mmol) in one portion. The resulting mixture was stirred for 18 h at room temperature, concentrated in vacuo, and partitioned between ether and a minimum amount of water. The layers were separated, and the aqueous layer was treated with AcOH dropwise until the solution measured acidic by pH paper. The solution was concentrated in vacuo, dried under high vacuum, and the resulting carboxylic acid was used without further purification in the next step. To a solution of (*R,S*)-1-(1-(isoquinolin-5-yl)ethyl)piperidine-4-carboxylic acid (0.100 g, 0.350 mmol) in dry DMF (5 mL) were added EDCI (0.067 g, 0.350 mmol), HOBt (0.070 g, 0.420 mmol), and DIEA (0.061 mL, 0.352 mmol) followed by (3-fluorophenyl)methanamine (0.044 g, 0.352 mmol). The mixture was stirred overnight at room temperature, diluted with saturated NaHCO_3 , and extracted with EtOAc (2 \times). The combined organic extracts were washed with saturated NaCl (3 \times), dried (MgSO_4), then purified by silica gel flash chromatography (1–5% MeOH/DCM) to afford the final compound (0.02 g, 16%). ^1H NMR (400 MHz, chloroform- d) δ 9.19 (s, 1H), 8.47 (d, $J = 6.1$ Hz, 1H), 8.18 (d, $J = 6.1$ Hz, 1H), 7.62–7.93 (m, 2H), 7.42–7.62 (m, 1H), 7.10–7.42 (m, 1H), 6.64–7.10 (m, 3H), 5.98 (t, $J = 5.8$ Hz, 1H), 4.39 (d, $J = 5.9$ Hz, 2H), 4.02 (q, $J = 6.7$ Hz, 1H), 3.14 (m, 1H), 2.56–3.04 (m, 1H), 1.89–2.37 (m, 3H), 1.53–1.89 (m, 3H), 1.42 (d, $J = 6.6$ Hz, 3H). TOF ES+ MS: (M + H) 392.1. HPLC $t_R = 4.0$ min, >95% purity.

N-(3-Fluorobenzyl)-1-(1-(isoquinolin-1-yl)ethyl)piperidine-4-carboxamide (4d). To a solution of 27d (50 mg, 0.16 mmol) in MeOH (10 mL) was added NaOH (11 mg, 0.48 mmol), and the mixture was allowed to stir at 50 °C for 6 h. The solution was concentrated in vacuo and acidified with 4 M HCl in dioxane (5 mL). The solution was again concentrated in vacuo and allowed to dry overnight. The crude carboxylic acid was dissolved in DMF (10 mL), and EDCI (49 mg, 0.38 mmol), HOBt (43 mg, 0.32 mmol), DIEA (103 mg, 0.80 mmol), and 3-fluorobenzylamine (24 mg, 0.20 mmol) were added and allowed to stir at 23 °C for 16 h. The reaction was quenched with saturated NaHCO_3 (25 mL), washed with H_2O (2 \times 20 mL), brine (1 \times 20 mL), dried (MgSO_4), and concentrated in vacuo. The residue was purified by flash chromatography (1–4% MeOH/DCM) to furnish the desired material (23 mg, 37.1%) as a dark brown oil. ^1H NMR (400 MHz, chloroform- d) δ 8.66 (d, $J = 8.5$

H₂, 1H), 8.44 (d, *J* = 5.7 Hz, 1H), 7.79 (d, *J* = 8.1 Hz, 1H), 7.65 (t, *J* = 7.9 Hz, 1H), 7.59–7.49 (m, 2H), 7.09–6.96 (m, 2H), 6.92 (t, *J* = 8.3 Hz, 2H), 5.81 (dd, *J* = 7.5, 1.9 Hz, 1H), 4.40 (d, *J* = 5.8 Hz, 2H), 3.09 (d, *J* = 10.1 Hz, 1H), 2.91 (d, *J* = 11.5 Hz, 1H), 2.36–2.26 (m, 1H), 2.18–2.07 (m, 2H), 1.77 (dd, *J* = 8.5, 3.5 Hz, 3H), 1.53 (d, *J* = 6.7 Hz, 3H). TOF ES+ MS: (M + H) 392.2. HPLC *t_R* = 5.2 min, >95% purity.

(R)-1-(1-(Naphthalen-1-yl)ethyl)-N-(pyridin-3-ylmethyl)piperidine-4-carboxamide (5a). Coupling method A: 50% yield. ¹H NMR (400 MHz, chloroform-*d*) δ 8.48–8.51 (m, 2H), 7.83 (d, *J* = 7.8 Hz, 3H), 7.76 (s, 1H), 7.47–7.53 (m, 4H), 7.23–7.25 (m, 1H), 6.08 (s, 1H), 4.44–4.45 (m, 2H), 3.26 (d, *J* = 11.5 Hz, 1H), 3.04 (d, *J* = 11.5 Hz, 1H), 2.11–2.48 (m, 2H), 1.63–2.11 (m, 7H), 1.48 (s, 3m). TOF ES+ MS: (M + H) 374.2. HPLC *t_R* = 4.6 min, >95% purity.

(R)-1-(1-(Naphthalen-1-yl)ethyl)-N-(pyridin-4-ylmethyl)piperidine-4-carboxamide (5b). Coupling method A: 27% yield. ¹H NMR (400 MHz, chloroform-*d*) δ 8.51 (d, *J* = 5.1 Hz, 2H), 7.79–7.83 (3H), 7.71 (s, 1H), 7.43–7.54 (m, 3H), 7.13 (d, *J* = 5.1 Hz, 2H), 6.06 (t, *J* = 6.2 Hz, 1H), 4.43 (d, *J* = 6.1 Hz, 2H), 3.63 (q, *J* = 6.7 Hz, 1H), 3.17–3.20 (m, 1H), 2.92–2.95 (m, 1H), 1.96–2.16 (m, 4H), 1.65–1.91 (m, 3H), 1.47 (d, *J* = 6.6 Hz, 3H). TOF ES+ MS: (M + H) 374.2. HPLC *t_R* = 4.6 min, >95% purity.

(R)-N-(2-Methoxypyridin-4-yl)methyl-1-(1-(naphthalen-1-yl)ethyl)piperidine-4-carboxamide (5c). Coupling method B: 26% yield. ¹H NMR (400 MHz, chloroform-*d*) δ 8.38 (br s, 1H), 8.06 (d, *J* = 5.3 Hz, 1H), 7.69–7.91 (m, 3H), 7.58 (br s, 1H), 7.45 (m, 3H), 6.72 (m, 1H), 6.56 (s, 2H), 5.85 (br s, 1H), 4.36 (d, *J* = 6.0 Hz, 2H), 4.10 (m, 1H), 3.89 (s, 3H), 3.25 (m, 1H), 2.94 (m, 1H), 1.58–2.15 (m, 5H), 1.41 (m, 3H). TOF ES+ MS: (M + H) 404.1. HPLC *t_R* = 4.5 min, >95% purity.

(R)-N-(4-Chlorophenethyl)-1-(1-(naphthalen-1-yl)ethyl)piperidine-4-carboxamide (6a). Coupling method B: 33% yield. ¹H NMR (400 MHz, chloroform-*d*) δ 8.41 (d, *J* = 7.5 Hz, 1H), 7.83 (dd, *J* = 7.1, 2.1 Hz, 1H), 7.72 (d, *J* = 8.2 Hz, 1H), 7.54 (m, 1H), 7.29–7.50 (m, 3H), 7.13–7.33 (m, 3H), 6.86–7.18 (m, 2H), 5.41 (s, 1H), 4.08 (s, 1H), 3.45 (q, *J* = 6.8 Hz, 1H), 3.18 (d, *J* = 11.2 Hz, 1H), 2.76–2.98 (m, 1H), 2.38–2.76 (m, *J* = 6.8 Hz, 2H), 1.52–2.16 (m, 7H), 1.45 (d, *J* = 6.8 Hz, 3H). TOF ES+ MS: (M + H) 421.1. HPLC *t_R* = 6.0 min, >95% purity.

(R)-N-(3-Fluorophenethyl)-1-(1-(naphthalen-1-yl)ethyl)piperidine-4-carboxamide (6b). Coupling method B: 36% yield. ¹H NMR (400 MHz, chloroform-*d*) δ 8.42 (d, *J* = 7.8 Hz, 1H), 7.77–8.04 (m, 1H), 7.73 (d, *J* = 8.2 Hz, 1H), 7.48–7.65 (m, 1H), 7.32–7.48 (m, 3H), 7.18–7.32 (m, 1H), 6.65–6.99 (m, 3H), 5.42 (s, 1H), 4.08 (d, *J* = 5.9 Hz, 1H), 3.37–3.56 (m, 1H), 3.19 (d, *J* = 11.2 Hz, 1H), 2.78–2.90 (m, 1H), 2.77 (s, 1H), 1.87–2.09 (m, 5H), 1.54–1.86 (m, 4H), 1.45 (d, *J* = 6.6 Hz, 3H). TOF ES+ MS: (M + H) 405.2. HPLC *t_R* = 5.8 min, >95% purity.

N-(3-Fluorobenzyl)-1-(1,2,3,4-tetrahydrophenanthren-4-yl)piperidine-4-carboxamide (7). To a solution of 33 (97 mg, 0.23 mmol) in THF/MeOH/H₂O (3:1:1) (7 mL) at 0 °C was added LiOH (19 mg, 0.45 mmol), and the mixture was allowed to stir at room temperature for 16 h. The reaction mixture was concentrated in vacuo, acidified using HCl–dioxane, and crystallized with the addition of EtOAc (5 mL). The product was filtered to furnish the carboxylic acid (65 mg, 70%) as a white solid. This acid was carried forward without purification and was dissolved (63 mg, 0.2 mmol) in dry DMF (5 mL), followed by EDCI (41 mg, 0.27 mmol), HOBt (37 mg, 0.27 mmol), DIEA (133 mg, 1.03 mmol), and 3-fluorobenzylamine (28 mg, 0.23 mmol), and the reaction mixture was allowed to stir at room temperature for 16 h. The reaction mixture was then diluted with EtOAc, quenched with saturated NaHCO₃, washed with H₂O (2 × 10 mL), saturated NaCl (1 × 10 mL), dried (MgSO₄), and concentrated in vacuo. The residue was purified by silica gel flash chromatography (40–60% EtOAc/Hex) to furnish 7 (26 mg, 30%) as a dark oil. ¹H NMR (400 MHz, chloroform-*d*): δ 8.37 (d, *J* = 8.4 Hz, 1H), 7.74 (d, *J* = 8.0 Hz, 1H), 7.63 (d, *J* = 8.4 Hz, 1H), 7.40 (dt, *J* = 21.1, 7.2 Hz, 2H), 7.24 (d, *J* = 4.5 Hz, 2H), 7.16 (d, *J* = 8.4 Hz, 1H), 6.95 (dd, *J* = 28.2, 8.1 Hz, 3H), 5.68 (s, 1H), 4.46 (t, *J* = 4.4 Hz, 1H), 4.39 (d, *J* = 5.8 Hz, 2H), 3.02–2.87 (m, 2H), 2.84–2.74 (m, 1H), 2.58 (ddd, *J* = 14.2, 9.9, 4.3 Hz, 2H), 2.33 (t, *J* = 10.7 Hz, 1H), 2.27–2.14 (m, 1H),

2.08 (ddt, *J* = 11.7, 8.0, 3.9 Hz, 1H), 2.01–1.91 (m, 1H), 1.85 (d, *J* = 10.5 Hz, 1H), 1.74 (dd, *J* = 10.8, 5.5 Hz, 2H), 1.61 (d, *J* = 12.1 Hz, 1H), 1.42–1.30 (m, 1H). TOF ES+ MS: (M + H) 417.2. HPLC *t_R* = 5.7 min, >95% purity.

2-Methoxy-1-(naphthalen-1-yl)ethanone (9c). 2-Methoxyacetonitrile 8c (0.25 mL, 3.33 mmol) was dissolved in a 250 mM solution of naphthalen-1-ylmagnesium bromide (20 mL, 5.0 mmol) in THF and stirred for 14 h at room temperature. 2 M HCl (10 mL) was added, and this was stirred at room temperature for 8 h. At this time, material was extracted with a 1:1 solution EtOAc/Et₂O, dried with anhydrous MgSO₄, filtered, and the filtrate was concentrated in vacuo. The residue was purified by flash chromatography (20 g silica, 5–20% EtOAc/Hex) to give the desired product (118 mg, 18%). ¹H NMR (500 MHz, chloroform-*d*) δ 8.66 (d, *J* = 8.6 Hz, 1H), 8.05 (d, *J* = 8.2 Hz, 1H), 7.91 (d, *J* = 8.1 Hz, 1H), 7.86 (d, *J* = 7.2 Hz, 1H), 7.64 (t, *J* = 7.7 Hz, 1H), 7.61–7.55 (m, 1H), 7.53 (t, *J* = 7.7 Hz, 1H), 4.74 (s, 2H), 3.57 (s, 3H).

(±)-1-(Naphthalen-1-yl)propan-1-ol (10a). 1-(Naphthalen-1-yl)propan-1-one 9a (100 mg, 0.54 mmol), prepared from nitrile 8a by the literature method,¹⁷ was dissolved in anhydrous THF (1 mL) in dry glassware and cooled to –78 °C. LAH (1 M in THF, 0.27 mL, 0.27 mmol) was added dropwise to the solution. The mixture was allowed to warm to room temperature and stirred for 4 h or until complete by TLC. The reaction was then worked up according to the Fieser method,⁵ and the resulting precipitate was filtered off. The filtrate was collected and concentrated in vacuo. The residue was then purified by flash chromatography (15 g silica, 20% EtOAc/Hex) to provide the desired product (85 mg, 85%). ¹H NMR (500 MHz, chloroform-*d*) δ 8.13 (d, *J* = 7.8 Hz, 1H), 7.94–7.89 (m, 1H), 7.81 (d, *J* = 8.2 Hz, 1H), 7.65 (d, *J* = 7.1 Hz, 1H), 7.57–7.47 (m, 3H), 5.44–5.34 (m, 1H), 2.32 (s, 1H), 2.09–2.00 (m, 1H), 1.99–1.89 (m, 1H), 1.06 (t, *J* = 7.4 Hz, 3H).

(±)-2-Methoxy-1-(naphthalen-1-yl)ethanol (10c). 2-Methoxy-1-(naphthalen-1-yl)ethanone 9c (118 mg, 0.59 mmol) was dissolved in anhydrous Et₂O (6 mL) in an ice bath, and a 1 M (in THF) solution of LAH (0.59 mL, 0.59 mmol) was added under N₂. This was stirred at room temperature for 3 h, at which time the Fieser workup⁵ was employed. Precipitate was filtered off and the filtrate concentrated in vacuo to give the desired product as an oil (104 mg, 87%) used without further purification. ¹H NMR (500 MHz, chloroform-*d*) δ 8.09 (d, *J* = 8.3 Hz, 1H), 7.93–7.89 (m, 1H), 7.83 (d, *J* = 8.2 Hz, 1H), 7.79 (d, *J* = 7.1 Hz, 1H), 7.58–7.50 (m, 3H), 5.75 (dd, *J* = 8.9, 2.5 Hz, 1H), 3.80 (dd, *J* = 10.1, 2.8 Hz, 1H), 3.57 (dd, *J* = 9.9, 9.0 Hz, 1H), 3.50 (s, 3H), 3.30 (bs, 1H).

(±)-Ethyl 1-(1-(Naphthalen-1-yl)propyl)piperidine-4-carboxylate (11a). 1-(Naphthalen-1-yl)propan-1-ol 10a (326 mg, 1.75 mmol) was dissolved in DCM (4 mL) at 0 °C with 3 Å molecular sieves. DIEA (0.92 mL, 5.25 mmol) was added, and with continuous stirring at 0 °C, Ms₂O (396 mg, 2.27 mmol) was added dropwise. The solution was stirred for 40 min at 0 °C, at which point ethyl piperidine-4-carboxylate (1.62 mL, 10.5 mmol) was added. The mixture was then stirred for 48 h at room temperature. At that time, EtOAc was added and washed with 10% aqueous Na₂CO₃ (3 × 25 mL). The organic layer was then dried (MgSO₄), filtered, and removed in vacuo. Purification was accomplished via flash chromatography (20 g silica, gradient 0–40% EtOAc/Hex) to give the desired product (480 mg, 84%) as a slightly yellow oil. ¹H NMR (500 MHz, chloroform-*d*) δ 8.48 (bs, 1H), 7.90–7.86 (m, 1H), 7.78 (d, *J* = 8.1 Hz, 1H), 7.54–7.43 (m, 4H), 4.14 (q, *J* = 7.1 Hz, 2H), 3.94 (bs, 1H), 3.29–3.16 (m, 1H), 2.87–2.75 (m, 1H), 2.27 (tt, *J* = 11.3, 4.1 Hz, 1H), 2.12–1.93 (m, 5H), 1.85–1.66 (m, 3H), 1.26 (t, *J* = 7.1 Hz, 3H), 0.70 (t, *J* = 7.3 Hz, 3H).

(±)-Ethyl 1-(2-Methoxy-1-(naphthalen-1-yl)ethyl)piperidine-4-carboxylate (11c). 2-Methoxy-1-(naphthalen-1-yl)ethanol 10c (104 mg, 0.51 mmol) was dissolved in DCM (4 mL) at 0 °C, and the following was added sequentially: 3 Å molecular sieves, DIEA (0.27 mL, 1.54 mmol), and Ms₂O (116 mg, 0.67 mmol). This was stirred for 40 min at 0 °C, at which time ethyl piperidine-4-carboxylate (0.48 mL, 3.09 mmol) was added. This was stirred for 48 h at room temperature. The material was extracted with EtOAc, and this was

washed with 10% Na₂CO₃ (3 × 25 mL). The organic layer was dried over MgSO₄, filtered, and the filtrate was concentrated in vacuo. The residue was purified by flash chromatography (20 g silica, 0–10% EtOAc/Hex gradient) to give the desired product (91 mg, 52%). ¹H NMR (500 MHz, chloroform-*d*) δ 8.41 (d, *J* = 8.2 Hz, 1H), 7.92–7.86 (m, 1H), 7.80 (d, *J* = 8.2 Hz, 1H), 7.63 (d, *J* = 7.0 Hz, 1H), 7.57–7.44 (m, 3H), 4.33–4.19 (m, 1H), 4.15 (q, *J* = 7.1 Hz, 2H), 3.95 (dd, *J* = 10.3, 6.2 Hz, 1H), 3.69 (dd, *J* = 10.3, 3.7 Hz, 1H), 3.33 (s, 3H), 3.32–3.25 (m, 1H), 2.86–2.77 (m, 1H), 2.38–2.23 (m, 2H), 2.14 (t, *J* = 10.2 Hz, 1H), 2.03–1.93 (m, 1H), 1.91–1.69 (m, 3H), 1.27 (t, *J* = 7.1 Hz, 3H).

(±)-1-(Naphthalen-1-yl)ethane-1,2-diol (13). 2-Hydroxy-1-(naphthalen-1-yl)ethanone **12** (200 mg, 1.07 mmol), prepared previously by the literature method,¹⁸ was dissolved in anhydrous THF (2 mL) and was cooled in an ice bath. 1 M LAH in THF (1.07 mL, 1.07 mmol) was slowly added dropwise to the solution. The mixture was then allowed to warm to room temperature and was stirred for 2 h. After this time, the reaction was worked up by the Fieser method,²⁷ the aluminum was filtered off, and the filtrate solvent was removed in vacuo to give a white solid. This was purified by flash chromatography (10 g silica, 50% EtOAc/Hex) to give the desired product (168 mg, 83%) as a white solid. ¹H NMR (500 MHz, DMSO-*d*₆) δ 8.16 (d, *J* = 8.3 Hz, 1H), 7.93 (d, *J* = 8.0 Hz, 1H), 7.82 (d, *J* = 8.1 Hz, 1H), 7.66 (d, *J* = 7.1 Hz, 1H), 7.57–7.48 (m, 3H), 5.44 (d, *J* = 4.2 Hz, 1H), 5.33 (dt, *J* = 7.7, 4.0 Hz, 1H), 4.87 (t, *J* = 5.8 Hz, 1H), 3.66 (ddd, *J* = 10.1, 6.0, 4.0 Hz, 1H), 3.50 (ddd, *J* = 11.3, 7.4, 5.9 Hz, 1H).

(±)-2-((tert-Butyldimethylsilyloxy)-1-(naphthalen-1-yl)ethanol (14). 1-(Naphthalen-1-yl)ethane-1,2-diol **13** (280 mg, 1.49 mmol) was dissolved in anhydrous DMF (8 mL), followed by imidazole (253 mg, 3.72 mmol) and TBSCl (247 mg, 1.64 mmol). This was stirred at room temperature for 4 h, after which time the mixture was partitioned between H₂O (25 mL) and EtOAc (25 mL) and extracted. The extract was washed with H₂O (1 × 20 mL) and brine (1 × 20 mL) and dried over MgSO₄ and concentrated in vacuo. The crude residue was then purified by flash chromatography (10% EtOAc/Hex) to give the silyl ether (445 mg, 99%) as a nearly colorless oil. ¹H NMR (500 MHz, methanol-*d*₄) δ 8.12 (d, *J* = 8.3 Hz, 1H), 7.82 (d, *J* = 8.1 Hz, 1H), 7.76–7.69 (m, 2H), 7.49–7.39 (m, 3H), 5.55 (dd, *J* = 6.6, 4.5 Hz, 1H), 4.94 (d, *J* = 4.2 Hz, 1H), 3.96–3.83 (m, 2H), 0.84 (s, 9H), –0.04 (s, 3H), –0.09 (s, 3H).

(±)-Ethyl 1-(2-((tert-Butyldimethylsilyloxy)-1-(naphthalen-1-yl)ethyl)piperidine-4-carboxylate (16). 2-((tert-Butyldimethylsilyloxy)-1-(naphthalen-1-yl)ethanol **14** (320 mg, 1.06 mmol) was dissolved in DCM (6 mL) with 3 Å molecular sieves, followed by DIEA (0.28 mL, 1.59 mmol). MsCl (0.10 mL, 1.27 mmol) was added dropwise, and the mixture was allowed to stir at room temperature for 3 h. Ethyl piperidine-4-carboxylate (0.82 mL, 5.29 mmol) was then added dropwise and the mixture stirred for 23 h at room temperature. A 1:1 solution of Et₂O/EtOAc (30 mL) was added. The solution was washed with aqueous 10% aqueous Na₂CO₃ (3 × 20 mL) and brine (1 × 15 mL), dried with anhydrous MgSO₄, filtered, and the filtrate was concentrated in vacuo. The crude residue was then purified by flash chromatography (20 g silica, 10% EtOAc/Hex) to give the desired product (276 mg, 59%) as an oil. ¹H NMR (500 MHz, chloroform-*d*) δ 8.41 (d, *J* = 7.8 Hz, 1H), 7.87 (d, *J* = 7.2 Hz, 1H), 7.77 (d, *J* = 8.1 Hz, 1H), 7.61 (d, *J* = 7.0 Hz, 1H), 7.51–7.41 (m, 3H), 4.17–4.11 (m, 3H), 4.11–4.07 (m, 1H), 3.91–3.86 (m, 1H), 3.42–3.33 (m, 1H), 2.85–2.76 (m, 1H), 2.35–2.24 (m, 2H), 2.12 (t, *J* = 11.3 Hz, 1H), 2.01–1.92 (m, 1H), 1.88–1.64 (m, 3H), 1.26 (t, *J* = 7.1 Hz, 3H), 0.81 (s, 9H), –0.12 (s, 3H), –0.15 (s, 3H).

(±)-*N*-(Benzo[*d*][1,3]dioxol-5-ylmethyl)-1-(2-((tert-butyl)dimethylsilyloxy)-1-(naphthalen-1-yl)ethyl)piperidine-4-carboxamide (17). Ethyl 1-(2-((tert-butyl)dimethylsilyloxy)-1-(naphthalen-1-yl)ethyl)piperidine-4-carboxylate **16** (100 mg, 0.23 mmol) was dissolved in ethanol (6 mL) and 7 M aqueous NaOH (3 mL) and stirred at 40 °C for 3 h. The mixture was then cooled to 0 °C and acidified (~pH 2) with concentrated HCl. The resulting white precipitate was collected over filter and dried under high vacuum overnight to give the desired carboxylic acid (70 mg, 75%) as a white powder. The crude solid was added to a solution of DIEA (0.059 mL,

0.338 mmol), EDCI (42.2 mg, 0.220 mmol), and HOBt (33.7 mg, 0.220 mmol) in anhydrous DMF (1 mL) over 3 Å molecular sieves. Piperonylamine (0.032 mL, 0.254 mmol) was added, and the mixture was allowed to stir for 32 h at room temperature. After this time, a 1:1 solution of Et₂O/EtOAc (25 mL) was added and washed with 10% aqueous Na₂CO₃ (3 × 20 mL) and brine (1 × 10 mL), dried with anhydrous MgSO₄, and concentrated in vacuo. The crude oil was purified by flash chromatography (25 g silica, 10% EtOAc/Hex) to give the desired product (46 mg, 50%) as an oil. ¹H NMR (500 MHz, chloroform-*d*) δ 8.39 (d, *J* = 7.4 Hz, 1H), 7.87 (d, *J* = 9.1 Hz, 1H), 7.77 (d, *J* = 8.2 Hz, 1H), 7.61 (d, *J* = 6.9 Hz, 1H), 7.53–7.39 (m, 3H), 6.80–6.69 (m, 3H), 5.96 (s, 2H), 5.73 (bs, 1H), 4.35 (d, *J* = 5.6 Hz, 2H), 4.17–4.05 (m, 2H), 3.88 (dd, *J* = 10.5, 4.0 Hz, 1H), 3.46 (d, *J* = 11.1 Hz, 1H), 2.85 (d, *J* = 11.3 Hz, 1H), 2.28 (t, *J* = 10.7 Hz, 1H), 2.19–2.09 (m, 1H), 2.09–2.01 (m, 1H), 1.95–1.72 (m, 4H), 0.81 (s, 9H), –0.12 (s, 3H), –0.15 (s, 3H).

1-(Naphthalen-1-yl)-2-phenylethanone (19). 1-Naphthonitrile **18** (1.00 g, 6.53 mmol) was dissolved in anhydrous Et₂O (20 mL) in dry glassware, followed by the addition of benzylmagnesium chloride (7.83 mL, 7.83 mmol) under N₂. This was stirred at room temperature for 18 h. At this time, 1 M HCl was added (5 mL) and the mixture was stirred at 90 °C for 35 min (during which time it was necessary to add more Et₂O), then allowed to cool to room temperature, at which point material was extracted by EtOAc/Et₂O, dried with anhydrous MgSO₄ and the filtrate was concentrated in vacuo. The resulting residue was purified by flash chromatography (20 g silica, 10% EtOAc/Hex) to give the desired ketone (1.35 g, 84%). ¹H NMR (500 MHz, chloroform-*d*) δ 8.60 (d, *J* = 8.8 Hz, 1H), 8.00 (ddd, *J* = 9.8, 7.1, 1.1 Hz, 2H), 7.90 (d, *J* = 7.3 Hz, 1H), 7.62–7.50 (m, 3H), 7.38–7.28 (m, 5H), 4.41 (s, 2H).

(±)-Dimethyl 1-(1-(Naphthalen-1-yl)-2-phenylethyl)pyridine-4,4(1H)-dicarboxylate (21). Dimethyl 2,2-bis((1,3-dioxolan-2-yl)methyl)malonate (578 mg, 1.90 mmol) was dissolved in a 1:1 mixture of THF (10 mL) to 10% aqueous HCl (10 mL) and stirred at room temperature for 18 h. At this time, the reaction was neutralized with solid NaHCO₃ and a solution of 1-(naphthalen-1-yl)-2-phenylethanamine **20** (446 mg, 1.80 mmol), prepared previously by the literature method¹⁹ from **19**, in THF (6 mL) was added. The mixture was stirred at room temperature for 20 h. At this time, the solution was extracted with EtOAc (2 × 50 mL) and the combined extracts were dried over anhydrous MgSO₄ and the filtrate was concentrated in vacuo. The residue was then purified via flash chromatography (15 g silica, 15% EtOAc/Hex) to give the desired condensed product (470 mg, 58%) as a yellow oil. ¹H NMR (300 MHz, chloroform-*d*) δ 7.92–7.85 (m, 3H), 7.66 (d, *J* = 0.9 Hz, 1H), 7.57–7.48 (m, 3H), 7.35–7.26 (m, 5H), 6.08 (d, *J* = 8.5 Hz, 2H), 5.21 (dd, *J* = 4.8, 9.7 Hz, 1H), 4.69 (d, *J* = 8.5 Hz, 2H), 3.72 (s, 6H), 3.56–3.35 (m, 2H).

(±)-Dimethyl 1-(1-(Naphthalen-1-yl)-2-phenylethyl)pyridine-4,4-dicarboxylate (22). Dimethyl 1-(1-(naphthalen-1-yl)-2-phenylethyl)pyridine-4,4(1H)-dicarboxylate **21** (80 mg, 0.187 mmol) was dissolved in N₂-sparged MeOH (5 mL), and 10% Pd/C was added. This was mixed under 40 psi of H₂ for 8 h at room temperature. This was then filtered through Celite and the filtrate concentrated in vacuo to give the desired product (57 mg, 71%) without further purification. ¹H NMR (500 MHz, chloroform-*d*) δ 8.51 (bs, 1H), 7.87–7.79 (m, 1H), 7.71 (d, *J* = 8.2 Hz, 1H), 7.50–7.43 (m, 2H), 7.29 (bs, 2H), 7.10–7.01 (m, 3H), 6.82 (bs, 2H), 4.13 (s, 1H), 3.74 (s, 6H), 3.44 (dd, *J* = 13.5, 4.6 Hz, 1H), 3.17 (dd, *J* = 13.5, 9.3 Hz, 1H), 2.72 (bs, 2H), 2.51 (bs, 2H), 2.29–2.08 (m, 4H).

(±)-Methyl 1-(1-(Naphthalen-1-yl)-2-phenylethyl)pyridine-4-carboxylate (23). Dimethyl 1-(1-(naphthalen-1-yl)-2-phenylethyl)pyridine-4,4-dicarboxylate **22** (103 mg, 0.24 mmol) was dissolved in anhydrous DMF (3 mL), and NaCN (17.6 mg, 0.36 mmol) was added to the solution. This was stirred at 145 °C for 16 h. The mixture was allowed to cool. H₂O was added, and material was extracted with EtOAc (3 × 50 mL). The combined organic extracts were dried with anhydrous MgSO₄ and concentrated in vacuo. The resulting residue was purified via flash chromatography (10 g silica, 20% EtOAc/Hex) to give the desired monoester (38 mg, 43%). ¹H NMR (500 MHz, chloroform-*d*) δ 8.49 (s, 1H), 7.83 (dt, *J* = 6.9, 3.5

H₂, 1H), 7.72 (d, *J* = 8.5 Hz, 1H), 7.47 (dt, *J* = 6.4, 3.3 Hz, 2H), 7.37–7.22 (m, 2H), 7.11–6.99 (m, 3H), 6.89 (s, 2H), 4.27 (s, 1H), 3.68 (s, 3H), 3.46 (dd, *J* = 13.6, 4.9 Hz, 1H), 3.31 (s, 1H), 3.20 (dd, *J* = 13.5, 9.1 Hz, 1H), 2.90 (d, *J* = 11.5 Hz, 1H), 2.28 (tt, *J* = 11.2, 4.0 Hz, 1H), 2.22–2.04 (m, 2H), 1.93 (d, *J* = 13.1 Hz, 1H), 1.84–1.66 (m, 3H).

1-(Quinolin-8-yl)ethanol (27a). To a -78°C solution of quinoline-8-carbaldehyde **26a** (0.5 g, 3.18 mmol) in dry THF under N₂ was added methylmagnesium chloride (3.82 mL, 3.82 mmol) dropwise. The resulting mixture was stirred 30 min before warming to room temperature. NH₄Cl was added, and the mixture was stirred for 10 min before diluting with EtOAc/Et₂O and washing with saturated NaCl and drying over MgSO₄. The residue was purified by flash chromatography (10–40% EtOAc/Hex) to afford the desired compound (0.435 g, 79%). ¹H NMR (400 MHz, chloroform-*d*) δ 8.84 (dd, *J* = 4.3, 1.9 Hz, 1H), 8.18 (dd, *J* = 8.3, 1.9 Hz, 1H), 7.72 (dd, *J* = 8.1, 1.6 Hz, 1H), 7.32–7.62 (m, 3H), 6.09 (s, 1H), 5.44 (q, *J* = 6.7 Hz, 1H), 1.73 (dd, *J* = 6.6, 0.4 Hz, 3H).

1-(Quinolin-5-yl)ethanol (27b). To a -78°C solution of quinoline-5-carbaldehyde **26b** (0.82 g, 5.2 mmol) in dry THF under N₂ was added methylmagnesium chloride (6.3 mL, 6.3 mmol) dropwise. The resulting mixture was stirred for 30 min before warming to room temperature. Saturated aqueous NH₄Cl was added, and the mixture was stirred for 10 min before being diluted with EtOAc/Et₂O, washed with saturated NaCl, and dried over MgSO₄. The residue was purified by silica flash chromatography (10–40% EtOAc/Hex) to afford the target compound (0.77 g, 86%) as a yellow oil. ¹H NMR (400 MHz, chloroform-*d*) δ 8.87 (d, *J* = 1.7 Hz, 1H), 8.53 (d, *J* = 8.6 Hz, 1H), 7.90–8.13 (m, 1H), 7.60–7.68 (m, 2H), 7.40 (dd, *J* = 8.6, 4.2 Hz, 1H), 5.59 (q, *J* = 6.5 Hz, 1H), 2.32 (br s, 1H), 1.65 (d, *J* = 6.5 Hz, 3H).

1-(Isoquinolin-5-yl)ethanol (27c). To a -78°C solution of isoquinoline-5-carbaldehyde **26c** (1.13 g, 7.19 mmol) in dry THF under N₂ was added methylmagnesium chloride (8.63 mL, 8.63 mmol) dropwise. The resulting mixture was stirred for 30 min before warming to room temperature. Saturated aqueous NH₄Cl was added, and the mixture was stirred 10 min before diluting with EtOAc/Et₂O. The organic layer was washed with saturated NaCl and dried over MgSO₄. Concentration provided a white solid which was triturated in ether, filtered, and dried under high vacuum to give 1-(isoquinolin-5-yl)ethanol **26c** (1.1 g, 88% yield). ¹H NMR (400 MHz, chloroform-*d*) δ 8.88 (d, *J* = 1.4 Hz, 1H), 8.48 (d, *J* = 7.8 Hz, 1H), 7.65 (m, 2H), 7.58 (m, 1H), 7.28–7.41 (m, 2H), 4.69 (q, *J* = 6.3 Hz, 1H), 1.49 (d, *J* = 6.3 Hz, 3H).

1-(Isoquinolin-1-yl)ethanol (27d). To a solution of 1-cyanoisoquinoline (301 mg, 1.96 mmol) in dry Et₂O (10 mL) at 0°C , 3.92 mL of 1 M MeMgBr (3.92 mmol) was added and allowed to stir for 3 h to produce a bright orange solution. The reaction was quenched with H₂O (15 mL) and 6 M HCl (5 mL) and stirred for 1 h at 80°C . The solution was basified with saturated NaHCO₃, extracted with Et₂O (2 \times 25 mL), dried over MgSO₄, and concentrated in vacuo. The residue was purified by silica flash chromatography (30% EtOAc/Hex) to furnish 1-(isoquinolin-1-yl)ethanol (304 mg, 91%) as a yellow oil. ¹H NMR (400 MHz, chloroform-*d*) δ 8.95 (d, *J* = 8.4 Hz, 1H), 8.57 (d, *J* = 5.5 Hz, 1H), 7.88–7.82 (m, 1H), 7.80 (d, *J* = 5.5 Hz, 1H), 7.69 (pd, *J* = 6.9, 1.3 Hz, 2H), 2.86 (s, 3H). This compound (304 mg, 1.78 mmol) was then dissolved in MeOH (6 mL), and NaBH₄ was added and the mixture was allowed to stir at 0°C for 18 h. The mixture was concentrated in vacuo and treated with saturated aqueous NH₄Cl. The solution was extracted with DCM (3 \times 10 mL), dried under MgSO₄, and concentrated in vacuo. The residue was purified by silica flash chromatography (30% EtOAc/Hex) to furnish the desired compound (226.5 mg, 73.6%) as a clear oil. ¹H NMR (400 MHz, chloroform-*d*) δ 8.43 (d, *J* = 5.7 Hz, 1H), 8.03 (d, *J* = 8.5 Hz, 1H), 7.86 (d, *J* = 8.2 Hz, 1H), 7.70 (ddd, *J* = 8.2, 7.0, 1.1 Hz, 1H), 7.66–7.54 (m, 2H), 5.58 (p, *J* = 5.7 Hz, 1H), 5.37–5.23 (m, 1H), 1.59 (d, *J* = 6.5 Hz, 3H).

Ethyl 1-(1-(Quinolin-8-yl)ethyl)piperidine-4-carboxylate (28a). To a 0°C solution of 1-(quinolin-8-yl)ethanol **27a** (0.47 g, 2.71 mmol) in dry DCM was added DIEA (1.05 g, 8.14 mmol) followed by Ms₂O (0.71 g, 4.10 mmol). The resulting mixture was stirred for 40 min at 0°C . Then ethyl piperidine-4-carboxylate (0.39 g,

1.27 mmol, 47% yield) was added in one portion. The resulting mixture was stirred overnight at room temperature, after which time the mixture was diluted with aqueous NaHCO₃ and extracted with DCM. The extracts were dried over MgSO₄, concentrated, and purified by flash chromatography (10–50% EtOAc/Hex) to provide **28a** as a clear oil (0.39 g, 47%). ¹H NMR (400 MHz, chloroform-*d*) δ 8.87 (d, *J* = 4.2, 1H), 8.53 (d, *J* = 8.6 Hz, 1H), 7.90–8.13 (m, 1H), 7.60–7.81 (m, 2H), 7.40 (dd, *J* = 8.6, 4.2 Hz, 1H), 5.59 (q, *J* = 6.5 Hz, 1H), 3.28–3.30 (m, 1H), 2.77–2.81 (m, 1H), 2.22–2.30 (m, 1H), 1.92–1.30 (m, 8H), 1.40 (d, *J* = 6.5 Hz, 3H), 1.23 (dd, *J* = 6.6, 0.4 Hz, 3H).

Ethyl 1-(1-(Quinolin-5-yl)ethyl)piperidine-4-carboxylate (28b). To a 0°C solution of 1-(quinolin-5-yl)ethanol **27b** (0.47 g, 2.70 mmol) in dry DCM was added DIEA (1.0 g, 8.14 mmol) followed by Ms₂O (0.71 g, 4.07 mmol). The resulting mixture was stirred for 40 min at 0°C , and then ethyl piperidine-4-carboxylate (0.70 g, 83% yield) was added in one portion. The resulting mixture was stirred overnight at room temperature, after which time the mixture was diluted with NaHCO₃ and extracted with DCM. The extracts were dried over MgSO₄, concentrated, and purified by flash chromatography (10–50% EtOAc/Hex) to give the desired compound (0.70 g, 83%) as a clear oil. ¹H NMR (400 MHz, chloroform-*d*) δ 8.87–8.91 (m, 1H), 7.98 (d, *J* = 8.5 Hz, 1H), 7.47–7.67 (m, 2H), 7.36 (m, 2H), 3.87–4.33 (m, 2H), 3.02 (d, *J* = 11.2 Hz, 1H), 2.76 (d, *J* = 11.2 Hz, 1H), 2.24 (m, 1H), 1.92–2.19 (m, 2H), 1.52–1.92 (m, 5H), 1.45 (dd, *J* = 6.7, 0.7 Hz, 3H), 1.21 (td, *J* = 7.1, 0.7 Hz, 3H).

Ethyl 1-(1-(Isoquinolin-5-yl)ethyl)piperidine-4-carboxylate (28c). To a 0°C solution of 1-(isoquinolin-5-yl)ethanol **27c** (0.47 g, 2.71 mmol) in dry DCM was added DIEA (1.05 g, 8.14 mmol) followed by Ms₂O (0.71 g, 4.07 mmol). The resulting mixture was stirred for 40 min at 0°C , and then ethyl piperidine-4-carboxylate (0.52 g, 1.67 mmol, 61.3% yield) was added in one portion. The resulting mixture was stirred overnight at room temperature, diluted with saturated NaHCO₃, and extracted with DCM. The extracts were dried over MgSO₄, concentrated, and purified by flash chromatography (10–50% EtOAc/Hex) to provide **27c** as a clear oil (0.52 g, 61% yield). ¹H NMR (400 MHz, chloroform-*d*) δ 9.22 (d, *J* = 0.9 Hz, 1H), 8.49 (dd, *J* = 6.1, 0.7 Hz, 1H), 8.20 (dd, *J* = 6.1, 1.0 Hz, 1H), 7.67–7.95 (m, 2H), 7.46–7.67 (m, 1H), 3.87–4.21 (m, 3H), 3.05 (d, *J* = 11.2 Hz, 1H), 2.74 (d, *J* = 11.2 Hz, 1H), 2.25 (tt, *J* = 11.2, 4.2 Hz, 1H), 1.95–2.17 (m, 2H), 1.57–1.95 (m, 4H), 1.43 (dd, *J* = 6.7, 0.7 Hz, 3H), 1.21 (t, *J* = 7.1 Hz, 3H).

Ethyl 1-(1-(Isoquinolin-1-yl)ethyl)piperidine-4-carboxylate (28d). To a solution of **27d** (215 mg, 1.24 mmol) in dry DCM were added DIEA (482 mg, 3.73 mmol) and Ms₂O (326 mg, 1.87 mmol), and the mixture was allowed to stir for 40 min at 0°C . To the solution, ethyl isonipicotate (586 mg, 3.73 mmol) was added dropwise, and the mixture was allowed to stir at 23°C for 18 h. The mixture was acidified using 6 M HCl (6 mL) and extracted with DCM (2 \times 15 mL). The aqueous layer was then basified using saturated NaHCO₃ (15 mL) and extracted with DCM (3 \times 15 mL). The organic layer was dried under MgSO₄ and concentrated in vacuo. The residue was purified by flash chromatography (10–50% EtOAc/Hex) to furnish the desired compound (62 mg, 16%) as a yellow oil. ¹H NMR (400 MHz, chloroform-*d*) δ 8.69 (d, *J* = 8.5 Hz, 1H), 8.45 (d, *J* = 5.7 Hz, 1H), 7.79 (d, *J* = 8.1 Hz, 1H), 7.67–7.61 (m, 1H), 7.57–7.47 (m, 2H), 4.36 (q, *J* = 6.7 Hz, 1H), 4.08 (q, *J* = 7.1 Hz, 2H), 2.25 (dt, *J* = 22.2, 8.2, 3.5 Hz, 2H), 2.11 (td, *J* = 11.3, 2.7 Hz, 1H), 1.88–1.75 (m, 2H), 1.75–1.67 (m, 2H), 1.65–1.61 (m, 1H), 1.52 (d, *J* = 6.7 Hz, 3H), 1.20 (t, *J* = 7.1 Hz, 3H).

1,2,3,4-Tetrahydrophenanthren-4-amine (30). To a solution of 2,3-dihydrophenanthren-4(1H)-one **29** (305 mg, 1.55 mmol) in isopropanol (50 mL) were added NaCNBH₃ (677 mg, 10.8 mmol) and NH₄(OAc) (4.831 g, 62.68 mmol), and the mixture was allowed to stir at reflux for 72 h under N₂ atmosphere. Approximately 50% of the solvent was evaporated, and the reaction mixture was extracted with DCM (3 \times 40 mL), dried under MgSO₄, and concentrated in vacuo to afford the desired compound (301 mg, 98%) as a dark oil, which was sufficiently pure to use in the next step. ¹H NMR (400 MHz, chloroform-*d*) δ 8.18 (d, *J* = 8.5 Hz, 1H), 7.79 (d, *J* = 8.1 Hz,

1H), 7.64 (d, $J = 8.5$ Hz, 1H), 7.53 (t, $J = 7.3$ Hz, 1H), 7.42 (t, $J = 7.4$ Hz, 1H), 7.19 (d, $J = 8.4$ Hz, 1H), 4.72 (s, 1H), 2.92 (dd, $J = 10.4, 5.7$ Hz, 2H), 2.15–1.84 (m, 4H).

Dimethyl 1-(1,2,3,4-Tetrahydrophenanthren-4-yl)pyridine-4,4(1H)-dicarboxylate (31). To a solution of dimethyl 2,2-bis((1,3-dioxolan-2-yl)methyl)malonate (464 mg, 1.53 mmol) in THF (10 mL) was added a 10% HCl solution (9.3 mL) dropwise. The reaction mixture was allowed to stir at room temperature for 16 h. The reaction mixture was neutralized with aqueous Na_2CO_3 . Amine **30** (301 mg, 1.53 mmol) was dissolved in THF (3 mL) and added dropwise to the reaction mixture. The pH was adjusted to ~ 5 using AcOH , and the reaction mixture was allowed to stir at room temperature for 72 h. The reaction mixture was quenched with saturated aqueous NaHCO_3 , extracted with EtOAc (2×15 mL), dried over MgSO_4 , and concentrated in vacuo. The residue was purified by silica flash chromatography (20% EtOAc/Hex) to furnish **31** (221 mg, 38%) as an oil. ^1H NMR (400 MHz, chloroform- d) δ 7.77 (d, $J = 7.9$ Hz, 2H), 7.71 (d, $J = 8.5$ Hz, 1H), 7.48 (t, $J = 7.5$ Hz, 1H), 7.41 (t, $J = 7.3$ Hz, 1H), 7.21 (d, $J = 8.4$ Hz, 1H), 6.05 (d, $J = 7.7$ Hz, 2H), 4.97 (s, 1H), 4.66 (d, $J = 7.8$ Hz, 2H), 3.68 (s, 5H), 3.13–2.74 (m, 4H), 2.28–2.08 (m, 2H).

Dimethyl 1-(1,2,3,4-Tetrahydrophenanthren-4-yl)piperidine-4,4-dicarboxylate (32). To a solution of **31** (221 mg, 0.59 mmol) in EtOAc (25 mL) was added PtO_2 (20 mg), and N_2 was bubbled through for 15 min. The mixture was placed under H_2 (40 psi) at room temperature for 5 h, and reaction progress was monitored by HPLC. The reaction mixture was filtered through Celite and concentrated in vacuo. The residue was then purified by silica flash chromatography (5–10% EtOAc/Hex) to furnish the desired compound (150 mg, 67%) as a yellow oil. ^1H NMR (400 MHz, chloroform- d) δ 8.37 (d, $J = 8.5$ Hz, 1H), 7.74 (d, $J = 7.7$ Hz, 1H), 7.63 (d, $J = 8.3$ Hz, 1H), 7.45–7.35 (m, 2H), 7.15 (d, $J = 8.4$ Hz, 1H), 4.43 (t, $J = 5.4$ Hz, 1H), 3.69 (s, 6H), 2.88 (t, $J = 5.4$ Hz, 1H), 2.82–2.76 (m, 1H), 2.54 (dd, $J = 7.3, 3.6$ Hz, 2H), 2.19–2.11 (m, 1H), 2.02 (dd, $J = 7.0, 3.4$ Hz, 1H), 1.94 (dd, $J = 7.3, 3.0$ Hz, 2H), 1.71 (dq, $J = 9.8, 5.3, 4.7$ Hz, 2H), 1.30–1.20 (m, 2H), 0.92–0.77 (m, 2H).

Methyl 1-(1,2,3,4-Tetrahydrophenanthren-4-yl)piperidine-4-carboxylate (33). To a solution of **32** (150 mg, 0.39 mmol) in DMF (10 mL) was added NaCN (29 mg, 0.59 mmol), and the mixture was allowed to stir at reflux for 16 h under N_2 atmosphere. The reaction mixture was cooled and diluted with EtOAc (10 mL), quenched with aqueous NaHCO_3 , and washed with saturated NaCl (2×10 mL). The extract was dried over MgSO_4 , concentrated in vacuo, and the residue was purified by silica flash chromatography (0–10% EtOAc/Hex) to furnish the desired compound (97 mg, 76%) as a yellow oil. ^1H NMR (400 MHz, chloroform- d) δ 8.40 (d, $J = 8.2$ Hz, 1H), 7.74 (d, $J = 7.8$ Hz, 1H), 7.63 (d, $J = 8.3$ Hz, 1H), 7.45–7.32 (m, 2H), 7.16 (d, $J = 8.4$ Hz, 1H), 4.44 (t, $J = 4.9$ Hz, 1H), 3.62 (s, 3H), 2.96–2.86 (m, 2H), 2.83–2.75 (m, 1H), 2.60–2.49 (m, 2H), 2.38–2.27 (m, 1H), 2.24–2.15 (m, 2H), 2.05–1.90 (m, 1H), 1.84 (d, $J = 14.0$ Hz, 1H), 1.74 (td, $J = 12.0, 10.7, 4.7$ Hz, 3H), 1.65 (d, $J = 14.5$ Hz, 1H), 1.34 (qd, $J = 12.1, 4.1$ Hz, 1H).

General Materials for Enzyme Purification and Kinetic Assays. SARS-CoV pET-15b-PLpro_(1541–1855) (cloned between the restriction sites *Bam*H I and *Bpu*1102 I) and the HCoV-NL63 pET-15b-PLP2_(1565–1894) (cloned between the restriction sites *Bam*H I and *Bpu*1102 I) were obtained from Dr. Susan Baker's lab at Loyola University Chicago, Stritch School of Medicine. For crystallization, SARS-CoV PLpro_(1541–1855) fused at the N-terminus to TEV protease cleavage sites and a 6 histidine tag was synthesized and codon optimized and cloned into pET11a using the restriction sites *Nde* I and *Bpu*1102 I by BioBasic Inc. Costar 96-well black microplates were purchased from Corning. Synthetic peptide substrate, Z-RLRGG-AMC, used for IC_{50} determination was purchased from Bachem. The *E. coli* expression strain BL21(DE3) was purchased from Novagen. LB medium components were purchased from BD Biosciences. The 5 mL HiTrap chelating HP column and the Superdex 200 were obtained from GE Healthcare, Life Sciences. Bradford reagent and BSA standard solution used for quantification of protein concentration were purchased from Bio-Rad. Human serum albumin (HSA, catalog no.

A9511, purity 97–99%) for serum shift assays was obtained from Sigma-Aldrich.

SARS-CoV PLpro and NL63-CoV PLP2 Expression and Purification. The expression plasmids containing SARS-CoV pET-15b-PLpro_(1541–1855), SARS-CoV pET-11a-PLpro_(1541–1855), and HCoV-NL63 pET-15b-PLP2_(1565–1894) were transformed into *E. coli* BL21(DE3) for protein expression. All purifications were performed at 4 °C with slight variations in the purification procedures. One liter of cells containing SARS-CoV pET-15b-PLpro_(1541–1855) wild type and mutants, SARS-CoV pET-11a-PLpro_(1541–1855), or HCoV-NL63 pET-15b-PLP2_(1565–1894) were grown for 24 h at 25 °C in medium containing 3 g of KH_2PO_4 , 6 g of Na_2HPO_4 , 20 g of tryptone, 5 g of yeast extract, 5 g of NaCl, pH 7.2, supplemented with 0.2% lactose, 0.6% glycerol, 0.05% glucose, and 50 $\mu\text{g}/\text{mL}$ carbenicillin. After growth, the cells were pelleted by centrifugation (18500g, 30 min at 4 °C) and an amount of ~ 12 g of cell pellet was resuspended in 50 mL of buffer A (20 mM Tris, pH 7.5, 500 mM NaCl, 10 mM imidazole) containing lysozyme and DNase I. The resuspended cells were lysed on ice via sonication using a 600 W model VCX ultrasonicator (7–8 min at 70% amplitude; 5.5 pulse on, 9.9 pulse off) or a 400 W 450 model digital sonifier cell disruptor (10 min at 60% amplitude; 5.5 pulse on, 9.9 pulse off). Cells debris were pelleted by centrifugation (30000g, 25 min, 4 °C).

For SARS-CoV PLpro WT and mutants (pET-15b-PLpro_(1541–1855) and pET-11a-PLpro_(1541–1855)), the clarified lysate was loaded at 2 mL/min onto a 5 mL HiTrap chelating HP column (GE Healthcare) charged with Co^{2+} and equilibrated with buffer A. Unbound proteins were washed with five column volumes (CV) of buffer A. Bound proteins were eluted with a linear gradient of 0–100% buffer B (20 mM Tris, pH 7.5, 500 mM NaCl, 500 mM imidazole), at 2 mL/min, followed by a 5 \times CV 100% buffer B wash. Fractions containing SARS-CoV PLpro were exchanged and concentrated into buffer C (20 mM Tris, pH 7.5, 20% glycerol, 10 mM DTT) to 5–10 mg/mL. Aliquots of 500 μL of the concentrated protein were flash frozen in liquid nitrogen for 10 min, then stored at -80 °C. HCoV-NL63 PLP2_(1565–1894) was purified by the same protocol as SARS-CoV PLpro except that a 5 mL HisTrap FF column (GE Healthcare) precharged with Ni^{2+} was used and 10 mM β -mercaptoethanol was included in the purification buffers.

For crystallization, the eluted fractions of the pET-11a-PLpro_(1541–1855) from the Co^{2+} column were concentrated and supplemented with 1 mg of TEV protease per 30 mg of PLpro and dialyzed for 18 h at 4 °C against 1 L ($\sim 1000\times$ dilution) of dialysis buffer (20 mM Tris, pH 7.5, 10% glycerol, 10 mM β -mercaptoethanol). Following dialysis the β -mercaptoethanol was removed by buffer exchange and the His-tagged TEV protease was removed by loading the sample onto a 5 mL HiTrap chelating HP column. Cleaved untagged SARS-CoV PLpro was obtained in the flow-through and concentrated to 25 mg/mL prior to loading onto a Superdex 200 26/60 gel filtration column equilibrated with buffer D (20 mM Tris, pH 7.5, 100 mM NaCl, and 10 mM DTT). The protein was eluted at a flow rate of 0.5 mL/min with equilibrium buffer, and the fractions containing SARS-CoV PLpro were concentrated to 6 and 12 mg/mL.

For all proteins, the protein concentration was determined by cuvette-based Bradford assay and purity was monitored by SDS-PAGE analysis and by calculating the specific activity at every step of the purification.

Determination of IC_{50} Values for Synthesized Compounds. The 100 μL inhibition assays were performed in triplicate in a 96-well plate format as previously described.^{14b} The final enzymes concentrations were 0.14 and 0.4 μM for SARS-CoV PLpro and HCoV-NL63 PLP2, respectively. The assays were performed at 25 °C, and the enzyme activity was monitored by measuring the PLP-mediated release of AMC from the RLRGG-AMC peptide substrate (50 μM), using the EnVision multimode plate reader from PerkinElmer.

Serum Shift Assays. Human serum albumin (HSA) was dissolved to a final concentration of 50 mg/mL in buffer containing 50 mM HEPES, pH 7.5, 2.5 mM DTT. Serum shift assays were performed by

determining the IC_{50} values for selected compounds as described above except that the assays contained 5%, 10%, or 20% HSA, where 40 mg/mL is 100%.^{25,26,28}

Counterscreen Assays for Selectivity against DUBs, USPs, and Cysteine Proteases. The NL63-HCoV PLP2 counterscreening assay was performed in a 100 μ L reaction volume including 400 nM enzyme, 100 μ M compound, and 50 μ M RLRGG-AMC substrate in assay buffer (50 mM HEPES, pH 7.5, 0.1 mg/mL BSA, 2 mM DTT). The assay was performed at 25 °C in triplicate for each inhibitor, and the enzyme activity was monitored as described above. The counterscreens with human USP and cysteine proteases were determined using purified enzymes available from Progenra, Inc. as part of their DUB screening service. The assays were performed in triplicate using 31.6 μ M compounds and Ub-rhodamine 110 as a substrate for USPs, Nedd8-EKL for DEN1, and commercially available fluorogenic peptide substrates for caspase 3 and cathepsin K.

Antiviral and Cytotoxicity Assays. SARS-CoV antiviral activity in infected Vero E6 cells was performed as previously described in a BSL-3 laboratory.^{14b} Briefly, Vero E6 cells were seeded into 96-well culture plates at 1×10^3 cells per well 24 h prior to infection with SARS-CoV. Cells were mock or SARS-CoV infected for 48 h in the presence of increasing concentrations of compounds. Upon incubation, cell viability was determined using Cell Titer-Glo luminescent cell viability assay (Promega). Experiments were performed twice in triplicate. Both the half maximal effective concentration (EC_{50}) and the 50% cytostatic concentration (CC_{50}) values were calculated using a four-parameter logistic equation by means of Sigma Plot 10 or GraphPad Prism software. Culturing and cell viability measurements of HEK 293 cells were performed as described above, in triplicate, 48 h after compound addition.

Liver Metabolism Studies. Compounds (1 μ M) were incubated with mouse liver microsomes (0.5 mg/mL) and NADPH in 0.1 M phosphate buffer at 37 °C as previously described.²⁹

Mutagenesis of Gln₂₇₀. The mutagenesis of Gln₂₇₀ to Ala, Glu, or Asp was performed by QuickChange site-directed mutagenesis as described by Zhen et al.³⁰ Mutant enzymes were purified as described above for the wild-type SARS-PLpro enzyme.

Crystallization of SARS-CoV PLpro in Complex with Inhibitors. Prior to crystallization, untagged SARS-CoV PLpro in 25 mM Tris, pH 7.5, 100 mM NaCl, 10 mM DTT at concentrations of 6 or 12 mg/mL was incubated with 2 mM inhibitor (dissolved in DMSO or ethanol) added to a 100 \times dilution and incubated overnight at 4 °C. Crystallization was performed at 20 °C using the sitting-drop vapor-diffusion method by mixing equal amounts of protein/inhibitor with reservoir solution containing 100 mM sodium citrate, pH 5.5, 40% (v/v) PEG 600. Crystals were soaked in cryosolution consisting of reservoir solution, 2 mM inhibitor, and 20% glycerol. Crystals were flash-frozen in liquid nitrogen and stored until synchrotron time was available. Crystals were transferred from liquid nitrogen into a stream of dry nitrogen gas at 100 K for X-ray data collection.

X-ray data were collected at the Life Sciences-Collaborative Access Team (LS-CAT) on beamline 21-ID-F at the Advanced Photon Source, Argonne National Laboratory. Data were processed and scaled using HKL2000. The SARS-CoV PLpro-3k and PLpro-3j complex crystallized as two monomers in the asymmetric unit. Crystals belong to space group C2 with unit cell dimensions of $a = 119$ Å, $b = 74$ Å, $c = 98$ Å, $\beta = 104^\circ$. The inhibitor-bound structures diffracted to resolutions of 2.1 and 2.5 Å for 3k and 3j, respectively. The initial phases were determined from molecular replacement solutions using the SARS-CoV PLpro-15g inhibitor complex structure (pdb:3MJS) as a search model and the MolRep³¹ program of the CCP4 suite.³² Model building and refinement was performed using the programs Refmac,³³ Phenix,³⁴ and Coot.³⁵ The final X-ray data processing and refinement statistics are summarized in Table 3. The final coordinates have been deposited in the Protein Data Bank under PDB code 4OW0 for PLpro-3k complex and PDB code 4OVZ for PLpro-3j complex.

■ ASSOCIATED CONTENT

Accession Codes

The atomic coordinates and structure factors have been deposited in the Protein Data Bank under code 4OW0 for PLpro-3k complex and code 4OVZ for PLpro-3j complex.

■ AUTHOR INFORMATION

Corresponding Authors

*S.D.L.: phone, (734) 615-0454; e-mail, sdlarsen@med.umich.edu.

*A.D.M.: phone, (765) 494-1924; e-mail, amesecar@purdue.edu.

Notes

The authors declare no competing financial interest.

■ ACKNOWLEDGMENTS

We gratefully acknowledge the synchrotron beamline personnel at the Advanced Photon Source (LS-CAT) 21-ID-F beamline. Use of the Advanced Photon Source was supported by the U.S. Department of Energy, Office of Science, Office of Basic Energy Sciences, under Contract DE-AC02-06CH11357. Use of the LS-CAT Sector 21 was supported by the Michigan Economic Development Corporation and the Michigan Technology Tri-Corridor (Grant 085P1000817). This work was partially supported by National Institutes of Health Grant AI085089 to A.D.M. and S.C.B. A.D.M. is also supported by a grant from the Walther Cancer Foundation. S.J.B. and M.P.A. were supported by University of Michigan Rackham Merit Fellowships. The authors also acknowledge support from the Purdue Center for Cancer Research DNA Sequencing and Macromolecular Crystallography shared resources.

■ ABBREVIATIONS USED

SARS, severe acute respiratory syndrome; CoV, coronavirus; SARS-CoV, severe acute respiratory syndrome coronavirus; HCoV, human coronavirus; MERS, Middle East respiratory syndrome; PLpro, papain-like protease; PLP2, papain-like protease 2; 3CLpro, chymotrypsin-like protease; HTS, high-throughput screening; Ub, ubiquitin; ISG15, interferon-induced stimulated gene 15; DUB, deubiquitinating enzyme; USP, ubiquitin specific protease; HSA, human serum albumin; PDB, Protein Data Bank

■ REFERENCES

- (1) Summary Table of SARS Cases by Country, 1 November 2002–7 August 2003. WHO: Geneva, August 15, 2003; http://www.who.int/csr/sars/country/2003_08_15/en/.
- (2) (a) van Boheemen, S.; Zaki, A. M.; Bestebroer, T. M.; de Graaf, M.; Victor, S.; Osterhaus, A. D.; Haagmans, B. L.; Fouchier, R. A. Genomic Analysis for a Newly Isolated Human Betacoronavirus Lineage 2C. Submitted Sep 26, 2012. (b) Bermingham, A.; Chand, M.; Brown, C.; Aarons, E.; Tong, C.; Langrish, C.; Hoschler, K.; Brown, K.; Galiano, M.; Myers, R.; Pebody, R.; Green, H.; Boddington, N.; Gopal, R.; Price, N.; Newsholme, W.; Drosten, C.; Fouchier, R.; Zambon, M. Severe respiratory illness caused by a novel coronavirus, in a patient transferred to the United Kingdom from the Middle East, September 2012. *Eurosurveillance* **2012**, *17* (40), No. pii=20290. (c) Pebody, R. G.; Chand, M. A.; Thomas, H. L.; Green, H. K.; Boddington, N. L.; Carvalho, C.; Brown, C. S.; Anderson, S. R.; Rooney, C.; Crawley-Boevey, E.; Irwin, D. J.; Aarons, E.; Tong, C.; Newsholme, W.; Price, N.; Langrish, C.; Tucker, D.; Zhao, H.; Phin, N.; Crofts, J.; Bermingham, A.; Gilgunn-Jones, E.; Brown, K. E.; Evans, B.; Catchpole, M.; Watson, J. M. The United Kingdom public health

response to an imported laboratory confirmed case of a novel coronavirus in September 2012. *Eurosurveillance* **2012**, *17* (40), 20292.

(3) de Groot, R. J.; Baker, S. C.; Baric, R. S.; Brown, C. S.; Drosten, C.; Enjuanes, L.; Fouchier, R. A.; Galiano, M.; Gorbalenya, A. E.; Memish, Z.; Perlman, S.; Poon, L. L.; Snijder, E. J.; Stephens, G. M.; Woo, P. C.; Zaki, A. M.; Zambon, M.; Ziebuhr, J. Middle East Respiratory Syndrome Coronavirus (MERS-CoV): Announcement of the Coronavirus Study Group. *J. Virol.* **2013**, *87*, 7790–7792.

(4) Kindler, E.; Jonsdottir, H. R.; Muth, D.; Hamming, O. J.; Hartmann, R.; Rodriguez, R.; Geffers, R.; Fouchier, R. A.; Drosten, C.; Muller, M. A.; Dijkman, R.; Thiel, V. Efficient Replication of the Novel Human Betacoronavirus EMC on Primary Human Epithelium Highlights Its Zoonotic Potential. *mBio* **2013**, *4* (1), No. e00611-12.

(5) van Boheemen, S.; de Graaf, M.; Lauber, C.; Bestebroer, T. M.; Raj, V. S.; Zaki, A. M.; Osterhaus, A. D.; Haagmans, B. L.; Gorbalenya, A. E.; Snijder, E. J.; Fouchier, R. A. Genomic characterization of a newly discovered coronavirus associated with acute respiratory distress syndrome in humans. *mBio* **2012**, *3* (6), No. e00473-12.

(6) (a) Perlman, S.; Zhao, J. Human coronavirus EMC is not the same as severe acute respiratory syndrome coronavirus. *MBio* **2013**, *4* (1), No. e00002-13. (b) Middle East Respiratory Syndrome Coronavirus (MERS-CoV): Update. WHO: Geneva, 2013.

(7) Danielsson, N.; ECDC Internal Response Team; Catchpole, M. Novel coronavirus associated with severe respiratory disease: case definition and public health measures. *Eurosurveillance* **2012**, *17* (39), No. pii=20282.

(8) Update: severe respiratory illness associated with a novel coronavirus—worldwide, 2012–2013. *Morbidity Mortality Wkly. Rep.* March 7, **2013**, *62* (Early Release).

(9) Tong, T. R. Drug targets in severe acute respiratory syndrome (SARS) virus and other coronavirus infections. *Infect. Disord.: Drug Targets* **2009**, *9* (2), 223–245.

(10) Harcourt, B. H.; Jukneliene, D.; Kanjanahaluethai, A.; Bechill, J.; Severson, K. M.; Smith, C. M.; Rota, P. A.; Baker, S. C. Identification of severe acute respiratory syndrome coronavirus replicase products and characterization of papain-like protease activity. *J. Virol.* **2004**, *78* (24), 13600–13612.

(11) (a) Barretto, N.; Jukneliene, D.; Ratia, K.; Chen, Z.; Mesecar, A. D.; Baker, S. C. The papain-like protease of severe acute respiratory syndrome coronavirus has deubiquitinating activity. *J. Virol.* **2005**, *79* (24), 15189–15198. (b) Lindner, H. A.; Fotouhi-Ardakani, N.; Lytvyn, V.; Lachance, P.; Sulea, T.; Menard, R. The papain-like protease from the severe acute respiratory syndrome coronavirus is a deubiquitinating enzyme. *J. Virol.* **2005**, *79* (24), 15199–15208.

(12) Lindner, H. A.; Lytvyn, V.; Qi, H.; Lachance, P.; Ziomek, E.; Menard, R. Selectivity in ISG15 and ubiquitin recognition by the SARS coronavirus papain-like protease. *Arch. Biochem. Biophys.* **2007**, *466* (1), 8–14.

(13) (a) Devaraj, S. G.; Wang, N.; Chen, Z.; Chen, Z.; Tseng, M.; Barretto, N.; Lin, R.; Peters, C. J.; Tseng, C. T.; Baker, S. C.; Li, K. Regulation of IRF-3-dependent innate immunity by the papain-like protease domain of the severe acute respiratory syndrome coronavirus. *J. Biol. Chem.* **2007**, *282* (44), 32208–32221. (b) Sun, L.; Xing, Y.; Chen, X.; Zheng, Y.; Yang, Y.; Nichols, D. B.; Clementz, M. A.; Banach, B. S.; Li, K.; Baker, S. C.; Chen, Z. Coronavirus papain-like proteases negatively regulate antiviral innate immune response through disruption of STING-mediated signaling. *PLoS One* **2012**, *7* (2), e30802.

(14) (a) Ratia, K.; Pegan, S.; Takayama, J.; Sleeman, K.; Coughlin, M.; Baliji, S.; Chaudhuri, R.; Fu, W.; Prabhakar, B. S.; Johnson, M. E.; Baker, S. C.; Ghosh, A. K.; Mesecar, A. D. A noncovalent class of papain-like protease/deubiquitinase inhibitors blocks SARS virus replication. *Proc. Natl. Acad. Sci. U.S.A.* **2008**, *105* (42), 16119–16124. (b) Ghosh, A. K.; Takayama, J.; Aubin, Y.; Ratia, K.; Chaudhuri, R.; Baez, Y.; Sleeman, K.; Coughlin, M.; Nichols, D. B.; Mulhearn, D. C.; Prabhakar, B. S.; Baker, S. C.; Johnson, M. E.; Mesecar, A. D. Structure-based design, synthesis, and biological evaluation of a series of novel and reversible inhibitors for the severe

acute respiratory syndrome-coronavirus papain-like protease. *J. Med. Chem.* **2009**, *52* (16), 5228–5240.

(15) Ghosh, A. K.; Takayama, J.; Rao, K. V.; Ratia, K.; Chaudhuri, R.; Mulhearn, D. C.; Lee, H.; Nichols, D. B.; Baliji, S.; Baker, S. C.; Johnson, M. E.; Mesecar, A. D. Severe acute respiratory syndrome coronavirus papain-like novel protease inhibitors: design, synthesis, protein–ligand X-ray structure and biological evaluation. *J. Med. Chem.* **2010**, *53* (13), 4968–4979.

(16) Ratia, K.; Saikatendu, K. S.; Santarsiero, B. D.; Barretto, N.; Baker, S. C.; Stevens, R. C.; Mesecar, A. D. Severe acute respiratory syndrome coronavirus papain-like protease: structure of a viral deubiquitinating enzyme. *Proc. Natl. Acad. Sci. U.S.A.* **2006**, *103* (15), 5717–5722.

(17) Kloetzel, M. C.; Wildman, W. C. Potential antimalarial compounds in the alpha-(1-dialkyl-aminoethyl)-1-naphthalenemethanol series. *J. Org. Chem.* **1946**, *11* (4), 390–394.

(18) Borman, R. A.; Coleman, R. A. 5-HT2B receptor antagonists. WO 2005 097113, Oct 20, 2005.

(19) Chow, K.; Fang, W. K.; Corpuz, E. G.; Gil, D. W.; Garst, M. E. Therapeutic fluoroethyl ethers. WO 2007 137029, Nov 29, 2007.

(20) Lee, H.; Cao, S.; Hevener, K. E.; Truong, L.; Gatz, J. L.; Patel, K.; Ghosh, A. K.; Johnson, M. E. Synergistic inhibitor binding to the papain-like protease of human SARS coronavirus: mechanistic and inhibitor design implications. *ChemMedChem* **2013**, *8* (8), 1361–1372.

(21) van der Hoek, L.; Sure, K.; Ihorst, G.; Stang, A.; Pirc, K.; Jebbink, M. F.; Petersen, G.; Forster, J.; Berkhout, B.; Uberla, K. Croup is associated with the novel coronavirus NL63. *PLoS Med* **2005**, *2* (8), e240.

(22) (a) Hodgson, E.; Philpot, R. M. Interaction of methylenedioxyphenyl (1,3-benzodioxole) compounds with enzymes and their effects on mammals. *Drug Metab. Rev.* **1974**, *3* (2), 231–301. (b) Anders, M. W.; Sunram, J. M.; Wilkinson, C. F. Mechanism of the metabolism of 1,3-benzodioxoles to carbon monoxide. *Biochem. Pharmacol.* **1984**, *33* (4), 577–580. (c) Barnette, W. E. The synthesis and biology of fluorinated prostacyclins. *CRC Crit. Rev. Biochem.* **1984**, *15* (3), 201–235.

(23) Wilkinson, C. F.; Murray, M.; Marcus, C. B. Interactions of methylenedioxyphenyl compounds with cytochrome-P-450 and effects on microsomal oxidation. *Rev. Biochem. Toxicol.* **1984**, *6*, 27–63.

(24) Guidance for Industry. Role of HIV Resistance Testing in Antiretroviral Drug Development. U.S. Department of Health and Human Services, Food and Drug Administration, Center for Drug Evaluation and Research (CDER): Rockville, MD, October 2007.

(25) Copeland, R. A. Determination of serum protein binding affinity of inhibitors from analysis of concentration-response plots in biochemical activity assays. *J. Pharm. Sci.* **2000**, *89* (8), 1000–1007.

(26) Peters, T., Jr. *All About Albumin: Biochemistry, Genetics, and Medical Applications*; Academic Press: San Diego, CA, 1996.

(27) Micovic, V. M.; Mihailovic, M. L. The reduction of acid amides with lithium aluminum hydride. *J. Org. Chem.* **1953**, *18* (9), 1190–1200.

(28) Schon, A.; del Mar Ingaramo, M.; Freire, E. The binding of HIV-1 protease inhibitors to human serum proteins. *Biophys. Chem.* **2003**, *105* (2–3), 221–230.

(29) Yestrepesky, B. D.; Xu, Y.; Breen, M. E.; Li, X.; Rajeswaran, W. G.; Ryu, J. G.; Sorenson, R. J.; Tsume, Y.; Wilson, M. W.; Zhang, W.; Sun, D.; Sun, H.; Larsen, S. D. Novel inhibitors of bacterial virulence: development of 5,6-dihydrobenzo[h]quinazolin-4(3H)-ones for the inhibition of group A streptococcal streptokinase expression. *Bioorg. Med. Chem.* **2013**, *21* (7), 1880–1897.

(30) Zheng, L.; Baumann, U.; Reymond, J. L. An efficient one-step site-directed and site-saturation mutagenesis protocol. *Nucleic Acids Res.* **2004**, *32* (14), e115.

(31) Vagin, A.; Teplyakov, A. Molecular replacement with MOLREP. *Acta Crystallogr., Sect. D: Biol. Crystallogr.* **2010**, *66* (Part 1), 22–25.

(32) The CCP4 suite: programs for protein crystallography. *Acta Crystallogr., Sect. D: Biol. Crystallogr.* **1994**, *50* (Part 5), 760–763.

(33) Winn, M. D.; Murshudov, G. N.; Papiz, M. Z. Macromolecular TLS refinement in REFMAC at moderate resolutions. *Methods Enzymol.* **2003**, *374*, 300–321.

(34) Adams, P. D.; Afonine, P. V.; Bunkoczi, G.; Chen, V. B.; Davis, I. W.; Echols, N.; Headd, J. J.; Hung, L. W.; Kapral, G. J.; Grosse-Kunstleve, R. W.; McCoy, A. J.; Moriarty, N. W.; Oeffner, R.; Read, R. J.; Richardson, D. C.; Richardson, J. S.; Terwilliger, T. C.; Zwart, P. H. PHENIX: a comprehensive Python-based system for macromolecular structure solution. *Acta Crystallogr., Sect. D: Biol. Crystallogr.* **2010**, *66* (Part 2), 213–221.

(35) Emsley, P.; Cowtan, K. Coot: model-building tools for molecular graphics. *Acta Crystallogr., Sect. D: Biol. Crystallogr.* **2004**, *60* (Part 12, Part 1), 2126–2132.